ER-anchored protein sorting controls the fate of two proteasome activators for intracellular organelle communication during proteotoxic stress

Gautier Langin[1,2], Margot Raffeiner[1], David Biermann[2], Mirita Franz-Wachtel[3], Daniela Spinti[4], Frederik Börnke[4,5], Boris Macek[3], Suayib Üstün[1,*]

[1] Faculty of Biology & Biotechnology, Ruhr-University Bochum, Bochum, Germany
[2] Center for Plant Molecular Biology (ZMBP), University of Tübingen, Tübingen, Germany
[3] Institute for Cell Biology, Department of Quantitative Proteomics, University of Tübingen, Tübingen, Germany Method section for MS/MS analysis
[4] Leibniz-Institute of Vegetable and Ornamental Crops (IGZ), Großbeeren, Germany
[5] Institute of Biochemistry and Biology, University of Potsdam, Potsdam, Germany

[*]Correspondence: suayb.uestuen@rub.de

Summary

Proteotoxic stress, characterized by the accumulation of damaged proteins, poses a significant challenge to cellular homeostasis. To mitigate proteotoxicity eukaryotes employ the proteasome that is regulated by proteasome activators, e.g. transcription factors that promote gene expression of proteasome subunits. As proteotoxicity originates in different compartments, cells need to perceive signals from various locations. Understanding which components integrate signals to address proteotoxicity is essential to develop strategies to cope with proteotoxicity but remain elusive. Here, we identify that the proteasome autoregulatory feedback loop acts as a gatekeeper to facilitate the communication between nucleus and chloroplast. We reveal that the ER-anchored protein sorting system (ERAPS) controls the proteasomal degradation or nuclear translocation of proteasome activators NAC53 and NAC78. While both transcription factors activate the proteasome gene expression, they repress photosynthesis-associated nuclear genes during proteotoxicity through association with a conserved cis-element. Our data implicate a general trade-off between proteasome function and energy metabolism unravelling an unprecedented mechanism of how eukaryotic cells cope with proteotoxicity. Collectively, our discoveries provide a novel conceptual framework in which the proteasome autoregulatory feedback loop coordinates subcellular proteostasis and the trade-off between growth and defence.

Main

Protein homeostasis, hereafter proteostasis, is defined as the synthesis of proteins and their regulated degradation. This intimate balance between protein synthesis and degradation is tightly regulated in all organisms to respond to several environmental stimuli[1,2]. Various perturbations can alter this equilibrium, leading to proteotoxic stress, the accumulation of aberrant proteins that cause ultimately irreversible cellular damage. These perturbations can range from ageing to pathological diseases such as Parkinson and Alzheimer as well as infection by pathogens[1,3]. The latter is a consequence of the onset and maintenance of defense responses during microbial infections and microbes' ability to manipulate proteostasis to their own benefit[3,4].

To mitigate deleterious effects due to excessive proteotoxic stress, cells employ various protein quality control machineries. One of the major protein quality control machineries across the tree of life is the ubiquitin-proteasome system (UPS). The UPS controls proteostasis through selective elimination of defective proteins and short-lived regulatory proteins[5]. To rapidly react to proteotoxic stress, all the constituents of the 26S proteasome are under a tight transcriptional control. All eukaryotic kingdoms possess transcription factors (TFs) required for proteasome gene activation[6]. Yeast utilizes Rpn4, mammals Nrf1/2 and plants the pair of NAC TFs (NAM, ATAF and CUC) NAC53/NAC78 as a conserved mechanism to cope with proteotoxicity. In yeast and animals, proteasome activators Rpn4 and Nrf1/2 have been shown to be UPS targets themselves, being degraded by the proteasome in the cytosol or ER[6]. Consequently, proteasome malfunction impairs their degradation leading to their stabilization and subsequent nuclear translocation to activate proteasome gene expression[6]. In plants, NAC78 mediates the transcriptional activation of proteasome promoters through the association with the proteasome regulatory cis element PRCE [TGGGC] [7]. In addition, loss of the NAC53/78 TF pair rendered plants hypersensitive to proteasome inhibition[8]. Therefore, a similar proteasome regulatory feedback loop has been proposed in plants[6]; however, to date, no evidence supports proteasomal removal of NAC53/78.

The involvement of the proteasome in various cellular pathways[9–11], suggests that the autoregulatory feedback loop is a central mechanism to precisely integrate and coordinate stress responses through proteotoxic stress sensing. Indeed, a growing body of evidence suggests that localized proteotoxic stress in organelles causes the activation of respective proteasome-mediated degradation pathways[12–16]. This implies a multi-layered signaling role of the proteasome in governing subcellular proteostasis. This aspect is particularly relevant for semi-autonomous organellar nuclear-encoded proteins, as their regulation also involves cytosolic

proteasomal degradation prior to organellar import[17,18]. As such, proteasome activators could act as gatekeepers of the communication between the nucleus and energy-producing organelles to maintain subcellular proteostasis. This could link the proteasome directly to energy metabolism as well as to the trade-off between growth and defense. However, to date it is unknown whether proteasome activators exert these functions.

Here we report that proteasome activators, TFs NAC53 and 78, orchestrate the communication between the nucleus and chloroplast during various stress conditions. We reveal that ER-anchored protein sorting (ERAPS) controls the proteasomal degradation and nuclear translocation of NAC53 and NAC78. While both TFs activate the proteasome gene expression, they repress photosynthesis-associated nuclear genes during proteotoxicity. The trade-off between proteasome activation and photosynthesis downregulation seems to be a general feature as it occurs in response to various environmental and developmental cues.

NAC53/78 are central integrators of various proteotoxic stress conditions

Proteotoxicity is triggered by a wide range of physicochemical stresses at different subcellular locations often leading to accumulation of proteins that are not imported into these organelles [17,19]. To understand whether proteasome activators might play a role in integrating signals from different locations, we used the proteasome activator mutant *nac53-1 78-1*[8] to disrupt cellular proteostasis through a variety of approaches (Fig.1a): (i) inhibiting the proteasome via bortezomib (BTZ) and bacterial infection with *Pseudomonas syringae pv. tomato DC3000* (Pst)[20,21], (ii) inhibiting the segregase CDC48 (CB-5083)[16,22], (iii) targeting HSP90 (GDA)[23], which plays a critical role in the import and degradation of chloroplastic/mitochondrial precursors, (iv) inducing ER stress with DTT and TM, and (v) targeting semi-autonomous organelles such as chloroplasts and mitochondria (Lin, Cml, MV)[23].

Perturbation of the proteasome by chemicals, bacteria, CDC48 inhibition and induced ER stress resulted in an increased susceptibility of the *nac53-1 78-1* mutant (Fig.1b), suggesting that both proteasome activators are involved in a general regulation of subcellular proteostasis. Strikingly, all other treatments perturbing organelle function (Lin, Cml, MV, GDA) resulted in increased tolerance of *nac53-1 78-1* (Fig.1b). Overall, our phenotypic screen implies that NAC53 and NAC78 integrate signals from different compartments to adjust their impact on plant response to stress.

104 **NAC53/78 are part of an autoregulatory proteasome feedback loop**

105 To elucidate how both TFs might integrate signals from different compartments and organelles,
106 we aimed to decipher their regulation through interactome analysis. Transgenic Arabidopsis
107 GFP-NAC53 and 78 lines (under the control of UBQ10 promoter) were only detectable for the
108 GFP fusion proteins upon proteasome inhibition by BTZ (Fig. 2,b), implying a high
109 proteasomal turnover of both NACs. Thus, we used *Agrobacterium*-mediated transient
110 expression in *Nicotiana benthamiana* to boost the expression of NACs for our interactome
111 studies. Transient expression of GFP-NAC53 and 78 (sTag construct) decorated the ER, being
112 consistent with the predicted transmembrane domain (TM) at the C-terminus of both proteins
113 (Fig. 2c and Extended Data Fig.1a). We additionally employed a chimeric construct (dTag-
114 NACs) tagged with fluorophores at the N and C-terminus following the TM domain (Extended
115 Data Fig.1a) to monitor subcellular interaction partners, as the RFP signal remained strictly in
116 the ER (Fig. 2d). BTZ treatment, stabilized all NAC constructs, supporting the notion of
117 NAC53/78 as proteasome targets and validating the functionality of the system in *N.*
118 *benthamiana* (Extended Data Fig.1b,c).

119 Next, we performed immuno-precipitation (IP) followed by tandem mass spectrometry
120 (MS/MS) with both constructs. We processed a total of 4 IP-MS/MS conditions for both NACs
121 among two experiments. We performed IP of sTag-NACs in mock conditions and at 8 hours
122 after bacterial infection, to induce proteotoxic stress (Extended data Fig.1D). In parallel, we
123 performed IP of dTag-NACs enriching for the N- or C-terminus end of the proteins, which
124 allowed us to characterize the interactome at a subcellular resolution (Extended data Fig.1E).
125 For our downstream analysis, we focused on the common interactors for both NACs. Out of
126 the 4 conditions we identified 245 unique *A. thaliana* orthologous proteins as interactor
127 candidates (Fig. 2e, Supplementary Table 1). The Gene Ontology (GO) annotations for cellular
128 components and the displayed enrichment for terms mainly associated with the proteasome
129 complex and plastid components (Extended Data Fig.1f). Investigating the SUBA5 annotation
130 of NAC53/78 interacting candidates, we found enrichment for following compartments: plastid,
131 peroxisome, Golgi, and ER (Extended Data Fig.1g). Further GO analysis for biological
132 processes revealed that possible candidates were enriched in proteins related to three main
133 biological process: proteolysis, trafficking and translation (Fig. 2f). We extracted the
134 corresponding proteins and performed a protein network analysis (Fig. 2g), highlighting the
135 presence of UPS components (Fig. 2g; Extended Data Fig.1h-k). However, proteasome
136 components were strongly reduced by bacterial infection and mainly enriched when targeting
137 the ER-anchored end of the TFs (C-ter IP) (Extended Fig.1h), indicating that both proteasome

regulators are degraded at the ER. The latter was further supported by the presence of several ER-associated degradation (ERAD) components in the interactome (Fig.2g and Extended Data Fig.1i). In summary, our interactome analysis validates the role of NAC53/78 as integrators of subcellular proteostasis disruptions, affirming their regulation by the proteasome autoregulatory feedback loop in plants.

ER-anchored protein sorting (ERAPS) regulates the subcellular fate of NAC53 & NAC78

Our interactome approach revealed that NAC53/78 associated with candidates that belong to the ERAD machinery, including membrane bound E3 ligase HRD1 and CDC48 (Fig. 2g and Extended data Fig.1i). To test whether ERAD is required to turnover the NACs, we took advantage of pharmacological drugs targeting individual steps in ERAD: we treated the GFP-NAC53 and GFP-NAC78 transgenic lines with CB-5083 and LS-102, inhibitors of CDC48 and HRD1 proteins, respectively[22,24]. We confirmed that previously uncharacterized LS-102 can efficiently inhibit both *A. thaliana* orthologs AtHRD1a and AtHRD1b *in vitro* (Extended data Fig. 2a,b). Similar to BTZ and CDC48, HRD1 inhibition led to a stabilization of both proteins; confirmed by confocal microscopy and immunoblotting (Fig. 3a,b). Collectively, these results indicate that NAC53/78 are targets of ERAD. Interaction studies of NACs with HRD1 isoforms revealed that GFP-NACs strongly associated with RFP-HRD1a/b in localization and co-IP experiments (Fig. 3c,d). The association was largely reduced upon deletion of the TM domain of both NAC TFs (ΔTM, Fig. 3c). Interestingly, loss of ER association led to a strong stabilization of the proteins, supporting ERAD-dependent turnover for both TFs (Fig. 3e). Subsequent *in vitro* ubiquitination assays using purified GST-HRD1a/b isoforms and MBP-NAC53/78 proteins confirmed that both NACs are ubiquitinated by HRDs, indicated by the appearance of higher molecular weight bands of MBP-NAC proteins (Fig. 3f). We could confirm the presence of ubiquitination marks at different sites via MS/MS analysis of the *in vitro* ubiquitination reactions (Extended Data Fig. 2c,e). In addition, ubiquitin marks were consistently inhibited by the addition of the inhibitor LS-102 to the *in vitro* ubiquitination assay (Extended data Fig.2f). The *in vitro* data was corroborated by the identification of several ubiquitination sites on NAC53 and 78 using *in vivo* IP-MS/MS analysis (Extended data Fig. 2d,e). This could be confirmed by performing ubiquitin IP on *N. benthamiana* leaves transiently expressing the NAC constructs (Extended data Fig. 2g). Mutation of identified lysine residues substantially reduced the association with anti-ubiquitin beads *in planta* (Extended data Fig. **2h,i**). Altogether, our *in vivo* and *in vitro* analysis demonstrate that NAC53 and NAC78 are directed to proteasomal degradation via ERAD through HRD1 ubiquitination.

172 During our analysis we observed that NAC53 and 78 responded different to the tested
173 inhibitors: while BTZ led to a strong signal in the nucleus, CDC48 inhibition led to the
174 appearance of cytoplasmic dot-like structures (Fig. 2a) that was not due to differences in drug
175 potency depending on the concentration of the drugs (Extended data Fig. 3a). Co-expression of
176 CDC48 isoform AtCDC48c with both NACs revealed that both proteins associated in dot-like
177 structures (Extended data Fig. 3b), suggesting that NAC53/78 accumulate at sites of CDC48
178 action upon CDC48 inhibition. Given the role of CDC48 in retro-translocation of ER proteins
179 to the cytosol we tested whether inhibition of its action can also perturb the subcellular sorting
180 of NACs comparing the GFP signal intensity in the nucleus and cytoplasm upon BTZ or CB-
181 5083 treatment. The proportion of the GFP signal in the nucleus was significantly lower when
182 plants were treated with CB-5083, supported by the lowered ratio of nucleus/cytoplasm GFP
183 intensity of plants subjected to the same treatment (Extended data Fig. 3c-f).
184 Together, our findings demonstrate the recycling of both NACs by the ERAD machinery,
185 regulated by HRD1 and CDC48, with the latter facilitating their nuclear translocation (Fig. 3g).
186 Thus, we propose to refer to this mechanism as ERAPS (ER-anchored protein sorting).
187
188 **The transcriptional landscape of proteotoxic stress**
189 To understand why the *nac53-1 78-1* mutant is more tolerant to organelle-directed proteotoxic
190 stress while it is hypersensitive to general proteotoxic stress we undertook a transcriptomic
191 analysis. To this end we exploited the *Pst*-mediated proteotoxic stress caused by the suppression
192 of proteasome activity and broad modification of chloroplast proteome[20,21,25]. Our analysis
193 revealed that *Pst* induced proteotoxic stress hallmarks were dependent on NAC53/78 (Fig.
194 4a,b,c, Extended data Fig.4a) and stabilized both NAC TFs in *N. benthamiana* and *A. thaliana*
195 (Fig. 4e,f). As such, this system is ideal to unveil the function of the proteasome autoregulatory
196 feedback loop in response to environmental perturbation. Next, we analysed the transcriptomic
197 profile of *nac53-1 78-1* infected with *Pst*, which revealed 945 differentially expressed genes
198 (DEGs). Strikingly, apart from the proteasome cluster most of the DEGs displayed a positive
199 Log2FC (Fig. 4g,h and Extended data Fig. 4a). This suggests that NAC53/78 are major
200 transcriptional repressors upon bacteria-induced proteotoxic stress. Further investigation of
201 which biological processes are enriched within the DEGs revealed photosynthesis,
202 glucosinolates, cell wall and auxin signalling as major terms (Fig. 4i). To obtain a global view
203 of the transcriptional landscape during proteotoxicity, we included two other datasets: (i)
204 transcriptome analysis of proteasome mutant *rpt2a-2* in response to *Pseudomonas syringae pv.*
205 *maculicola* (*Pma*) infection (Extended data Fig.4b-e) and (ii) previously characterized

206 transcriptome analysis on Col-0 plants upon MG132 treatments[8]. The comparison of all three
207 datasets allowed us to extract a core set of 538 DEGs present in the *nac53-1 78-1* dataset and
208 at least one of the other datasets (Fig. 4j and Supplementary Table 2). Extracting the genes
209 associated with these processes from the *nac53-1 78-1* 945 DEGs, we could define the core
210 transcriptional network associated with proteotoxic stress (Fig. 4l). This network is comprised
211 of 4 modules: the proteasome genes, a major cluster of photosynthesis associated nuclear genes
212 (PhANGs), glucosinolate and auxin signalling pathways (Fig. 4k,l). Only the proteasome and
213 photosynthesis cluster were present in all three datasets (Extended data Fig.4f). This suggests
214 that PhANGs transcriptional repression is a recurrent response to proteotoxic stress. Altogether
215 our analysis revealed a so far unidentified link between NAC53/78 and the transcriptional
216 regulation of PhANGs in response to proteotoxic stress.
217
218 **NAC53 and NAC78 coordinate the regulation of proteasome and photosynthesis gene**
219 **expression through the same cis-element**
220 The global transcriptional profile during proteotoxic stress indicates a strong link between
221 proteasome activation and repression of photosynthesis. Thus, we hypothesized NAC53/78 can
222 act as novel repressors of PhANGs. Detailed analysis of distinct photosynthetic processes
223 revealed that while many processes were downregulated during proteotoxic stress, loss of
224 NAC53/78 had a general effect on PhANGs transcriptional regulation (Extended data Fig. 5a).
225 Enrichment analysis for specific promoter cis-elements in the 4 gene clusters of the core
226 transcriptional network (Fig. 4k,l) revealed that the proteasome genes and PhANGs share a
227 common cis-element characterized by the PRCE-like [TGGGC] core motif (Fig. 5a). In line
228 with this, PRCE-like elements appeared homogeneously distributed among PhANGs promoters
229 and enriched close to the transcription starting site (Extended data Fig. 5b,c). We then extracted
230 the promoter regions of selected candidates, LHCa3 and PSAD1, (Fig. 5b), members of the
231 light harvesting complex I and photosystem I[26]. Performing electromobility shift assay
232 (EMSA), we could confirm that NAC53 and NAC78 directly bind to these elements (Fig. 5c),
233 dependent on the presence of their respective DNA recognition motif (Fig. 5c). Furthermore,
234 we confirmed the TGGGC motif as being the driver of this association, as mutated oligos were
235 unable to outcompete the association of NAC53/78 with the probes (Fig. 5d). Chromatin IP
236 followed by qPCR corroborated our findings, as both TFs were only able to associate to the
237 selected promoter regions when plants were challenged with bacteria-induced proteotoxic stress
238 (Fig. 5e). Performing luciferase reporter assays in protoplasts [27], we revealed that the PSAD1
239 promoter activity was consistently repressed by NAC53 and 78, which did not occur in *nac53-*

240 *1 78-1* mutant protoplasts (Extended data Fig. 5d). Deletion of the PRCE motif in PSAD1
241 abolished NAC78-mediated repression, while NAC53 led to an increase in promoter activity
242 (Extended data Fig. 5e). In contrast, LHCa3 promoter activity appeared to be rather induced by
243 NAC53 and unchanged by NAC78 (Extended data Fig. 5d), with NAC53-mediated activation
244 being dependent on the PRCE motif (Extended data Fig. 5e). This difference might be due to
245 the fact that both TFs are expressed without a TM domain, bypassing ERAPS, in a rather
246 artificial system. To circumvent this, we analysed the gene expression of *LHCa3* and *PSAD1* in
247 the transgenic NAC53 and 78 lines upon BTZ treatment. Proteasome inhibition in the
248 transgenic NAC53 and 78 lines partially enhanced the repression of PhANGs, supporting the
249 notion that NAC53/78 act as repressors of photosynthesis during proteotoxic stress (Extended
250 data Fig. 5f). In addition, both lines showed an increase in *PBA1* and *RPT2a* mRNA (Extended
251 data Fig. 5g), confirming that NAC53/78 can act concomitantly as transcriptional repressor and
252 activator. These results confirmed the importance of the PRCE-like element in PhANGs
253 promoters, suggesting that NAC53 and NAC78 possess the ability to modulate each other's
254 activity and highlights the complexity of the NAC53/78-PRCE regulatory module mediating
255 transcriptional repression of PhANGs and activation proteasome genes. To confirm that
256 NAC53/78 act indeed as novel repressors of photosynthesis we monitored the abundance of
257 photosynthesis proteins, PSII activity and photosynthetic pigment content upon bacteria-
258 induced proteotoxicity. To summarize, we detected that bacterial infection had a significantly
259 lesser impact on all measured photosynthesis readouts in the *nac53-1 78-1* double mutant
260 compared to Col-0 (Fig. 5f-j). Consistently with these findings, subjecting the NAC53/78
261 transgenics to constant proteasome inhibition resulted in strong developmental defect
262 (Extended data Fig.5h,i), suggesting that the role of NAC53/78 on photosynthesis repression is
263 not restricted to bacterial infection. Altogether, we demonstrate the unique ability of NAC53
264 and NAC78 to mediate activation and repression of target genes through the same PRCE
265 element. This makes them novel repressors of photosynthesis during proteotoxic stress and
266 explains our previous findings that the NAC mutant was more tolerant to organelle-directed
267 proteotoxic stress.
268

269 **The proteasome autoregulatory feedback loop monitors photosynthesis homeostasis**
270 **during stress responses**

271 Our results suggest that photosynthesis repression by NAC53/78 is a general feature of the
272 proteasome autoregulatory feedback loop to cope with proteotoxicity. In line with this, recent
273 evidence indicates that loss of proteasome function in a chloroplast import deficient mutant

274 improved photosynthesis due to a lack of chloroplast precursor protein degradation[28]. To
275 analyze to which extent NAC53/78 are involved in the response to chloroplast perturbation, we
276 investigated photosynthesis readouts upon BTZ and Lincomycin treatments in *nac53-1 78-1*
277 plants. All readouts (pigment content, PhANGs expression, PSII activity) were significantly
278 less impaired in *nac53-1 78-1* (Fig. 6a, b and Extended data Fig. 6a), suggesting that NAC53/78
279 are indeed monitoring PhANGs expression during chloroplast stress. We then repeated the
280 phenotypic screen introduced in Fig. 1 using the *hrd1a 1b* double mutant[29] to investigate the
281 direct involvement of the proteasome autoregulatory feedback loop in coordinating cellular
282 proteostasis and photosynthesis. Proteasome inhibition rendered the *hrd1a 1b* more tolerant in
283 comparison to Col-0 (Fig. 6c), which is consistent with its role in negatively regulating
284 NAC53/78 stability (Fig. 3g). In contrast, all other tested drugs or bacterial infection rendered
285 the *hrd1a 1b* mutant more susceptible (Fig. 6c,d). The reduced growth of *hrd1a 1b* upon
286 chloroplastic perturbations (Cml and Lin) are consistent with our previous results (Fig. 1b), as
287 stabilisation of NACs would lead to increased repression of PhANGs and growth reduction
288 (Extended data Fig. 5a, h,I). The impaired performance of *hrd1a 1b* upon CDC48 inhibition,
289 pathogen infection or ER stress induction might be due to the general function of HRDs in
290 ERAD[30]. Analysis of the photosystem II activity revealed a stronger reduction in the *hrd1a 1b*
291 double mutant (Extended data Fig. 6b) upon infection corroborating our findings that ERAPS
292 coordinates proteasome and photosynthesis through NAC53/78 stability. In addition, these data
293 suggest that organellar perturbation would lead the NAC53/78 activation. Indeed, subjecting
294 GFP-NACs transgenics to several organellar perturbators led to stabilization and nuclear
295 localization of both TFs (Extended data Fig. 6c). Taken together our analysis illustrates the
296 importance of the proteasome autoregulatory feedback loop in maintaining the fine equilibrium
297 of proteostasis to ensure normal response to proteotoxic stress and suggests that it is involved
298 in other biological contexts. To answer this, we performed a large-scale meta-transcriptomic
299 analysis using the recently developed Arabidopsis RNAseq data base[31]. Using our pipeline (see
300 methods and Supplementary Table 3) we investigated the correlation of transcript abundance
301 between the 54 genes encoding 26S proteasome subunits and the 68 PhANGs associated with
302 proteotoxic stress. We could observe that genes within the same cluster displayed a strong
303 positive correlation ($\rho \approx 0.6$ and $\rho \approx 0.5$ for 26S Proteasome and PhANGs, respectively).
304 Strikingly, analysing the relationship between the two clusters Proteasome vs. PhANGs showed
305 a significant negative correlation ($\rho \approx -0.4$) (Fig. 6e), supporting the notion that this is a general
306 phenomenon. To investigate this in more detail, we extracted 43 projects in which 26S
307 Proteasome and PhANGs appear transcriptionally co-regulated (Supplementary Table 3). From

308 these 43 projects, 35 displayed an opposite regulation for 26S Proteasome and PhANGs mRNA
309 level (Extended data Fig. 6d), confirming that both clusters undergo recurrent contrasting co-
310 regulation. Amongst them pathogen attack, abiotic stress (cold, dark, drought), circadian
311 rhythm, nutrient stress, hormone treatment (SA, auxin) as well as treatment with phytotoxins
312 (trans-chalcone) resulted in a negative correlation. It suggests that coordination of
313 PhANGs/proteasome is a general feature of plant stress responses and developmental processes.
314 Thus, the coordination of proteasome activation and PhANGs repression is a key feature of the
315 *A. thaliana* transcriptome in response to multiple biotic, abiotic, and developmental cues.
316

317 **Discussion**

318 Understanding how the proteasome can degrade proteins from different compartments and how
319 these different subcellular signals are integrated upon external cues and to maintain overall
320 proteostasis was a long-standing question. Our study discovered that the NAC53/78 module
321 acts as a gatekeeper to facilitate the communication between the chloroplast-proteasome-
322 nucleus during proteotoxic stress (Extended Data Fig. 7). We have identified ERAPS as the key
323 regulatory node of the proteasome autoregulatory feedback loop that shapes and maintains
324 subcellular proteostasis in plants. Considering this loop is mechanistically conserved across
325 kingdoms, similar control mechanisms of subcellular proteostasis are possible in yeast and in
326 animals[6]. Interestingly, connections between ER-anchored TFs and proteasome activation have
327 previously been observed in animals, whilst separate studies identified an indirect link between
328 proteasomal, and mitochondrial transcriptional regulation in yeast[19]. However, a unified
329 mechanism that explains the direct crosstalk between these seemingly disparate processes has
330 been lacking. This implies a divergence between yeast and plants on subcellular proteostasis
331 coordination.

332 Our findings highlight that subcellular proteostasis is governed by the ERAPS-dependent
333 autoregulatory pathway permitting a rapid integration of proteotoxic signals from various
334 compartments. As such, it allows the communication between different organelles such as
335 chloroplast or mitochondria with the nucleus, a process referred as retrograde signaling[32]. This
336 communication is essential to respond to sudden changes in the environment. Retrograde
337 signaling from mitochondria or chloroplast to the nucleus involves massive transcriptional
338 changes that in turn influence organelle function[33]. Some nuclear communicators have been
339 identified to mediate retrograde signaling[33]. However, to date, transcription factors GLK1 and
340 2, are the only known PhANGs activators[34], while putative repressors ABI4 and PTM could not
341 be verified as retrograde signaling components[35–38]. Here we have identified that plants have

evolved a dual-regulatory system through the proteasome autoregulatory feedback loop: the NAC53/78-PRCE module acts as a novel retrograde signaling component, repressing PhANGs expression and activating proteasome genes via the same cis-element during proteotoxic stress. In this scenario, (i) repression of PhANGs by NAC53/78 may be a strategy to cope with the excess of precursor accumulation due to proteasomal stress (Extended Data Fig. 7) which is corroborated by our findings that the *nac53-1 78-1* mutant is more tolerant to photosynthesis stress and HSP90 inhibition which activate NAC53/78 nuclear localization but also (ii) to counteract the overactivation of PhANGs by GLK1 that is degraded by the proteasome[39]. To our knowledge, a similar system has not been found in other multicellular organisms such as animals. However, findings in animals that connect proteasome activators and mitochondrial biogenesis[40], strongly suggest a tight link between proteoasome and energy metabolism in animals.

Various environmental perturbations impede the balance between protein translation, sorting and degradation resulting in proteotoxicity. Mounting evidence highlights a role for the proteasome in clearing organelle-associated proteins and immune components, mediating the growth-defense trade-off. Thus, it is essential to decipher how signals from different compartments and organelles are integrated to maintain proteostasis during various stress conditions. Our findings provide a new conceptual framework for understanding the integral role of the proteasome complex as a *bona fide* signalling hub, to manage cellular proteostasis under environmental stress. This framework could be potentially universally employed across various organisms to adapt to internal and external disruptions.

374 # FIGURE LEGENDS

375 **Fig. 1. NAC53/78 are central integrators of various proteotoxic stress conditions.**
376 (A) The role of the 26S Proteasome in degradation of proteins from distinct subcellular
377 compartments. Prime site of action of the several treatments used in this study: Blunt head
378 arrows indicate enzymatic activity suppression; pointed head arrows indicate trigger of
379 substrate accumulation.
380 (B) Fresh weight of seedlings grown under the indicated treatments at 10-14 day after
381 germination (dag). Fresh weight is expressed as a percentage of Col-0 mock conditions.
382 Boxplots colors refer to the genotype. Statistical significance is assessed by a Wilcoxon-Mann-
383 Whitney test (p values: n.s. > 0.05; * < 0.05; ** < 0.01). Every treatment has been repeated at
384 least twice with similar results.
385 (C) Bacterial density in Log10 Colony-Forming-Unit (CFU) per leaf cm^2. Statistical
386 significance is assessed by a Wilcoxon-Mann-Whitney test (p values: n.s. > 0.05; ** < 0.01).
387 Boxplots colors refer to the genotype as in panel B. The treatment has been repeated three times
388 with consistent results.
389 (B-C) Representative phenotypic pictures of Col-0 and *nac53-1 78-1* plants under several
390 treatments are included.
391
392 **Fig. 2. NAC53/78 are part of an autoregulatory proteasome feedback loop.**
393 (A) Confocal microscopy pictures of roots of GFP-NAC53/78 *Arabidopsis thaliana* transgenics
394 at 7dag exposed to mock or BTZ 10µM treatment for 3h. Treatments were repeated at least
395 three times with similar observations.
396 (B) Immunoblot analysis against GFP on crude extract of seedlings related to panel A. Ponceau
397 staining is used as loading control.
398 (C) Confocal microscopy pictures of transiently co-expressed sTag-NAC53/78 with
399 prom35S::RFP-HDEL or together in *N. benthamiana* epidermis cells. Pearson index (ρ)
400 represents co-localization index. Scale bars = 10µm
401 (D) Confocal microscopy pictures of transiently co-expressed sTag-NAC53/78 together or
402 dTag-NAC53/78 alone in *N. benthamiana* epidermis cells. Scale bars = 10µm
403 (E) Bar plots representing the number of significantly enriched proteins in the 4 IP-MS/MS
404 conditions for NAC53 only, NAC78 only and NAC53+NAC78 (Common).
405 (F) Cladogram of top 30 gene ontology (GO) terms for biological process (BP) enriched in the
406 list of *A. thaliana* ortholog proteins found from NAC53/78 common interactome.
407 (G) Protein network of the interacting candidates related to the GO BP terms annotated as
408 "Transport" and "Proteolysis" in panel F.
409
410 **Extended data Fig. 1. Deciphering the details of NAC53/78 interactome.**
411 (A) Chimeric NAC53/78 constructs generated in this study. Upstream promoter, fluorescent tag
412 and protein domain of interests are represented.
413 (B) Immunoblot against GFP on crude extracts of *N. benthamiana* leaves transiently expressing
414 sTag-NACs in addition to mock or 6h BTZ (10µM) treatment. Ponceau staining is used as
415 loading control.
416 (C) Immunoblot against GFP or RFP on crude extracts of *N. benthamiana* leaves transiently
417 expressing dTag-NACs in addition to mock or BTZ 10µM for 6h. Ponceau staining is used as
418 loading control.
419 (D) Immunoblot against GFP after immunoprecipitation (IP) with anti-GFP agarose beads on
420 *N. benthamiana* leaf extracts transiently expressing sTag-NACs after mock or *PstΔHopQ*
421 infection for 8h. The same samples were used for subsequent MS/MS analysis.
422 (E) Immunoblot against GFP or RFP after IP with anti-GFP or anti-RFP agarose beads on *N.*
423 *benthamiana* leaf extracts transiently expressing dTag-NACs. The same samples were used for
424 subsequent MS/MS analysis.

425 (F) Cladogram of top 30 GO terms for cellular components enriched in the list of *A. thaliana*
426 ortholog proteins found in NAC53/78 common interactome.
427 (G) Subcellular compartments enrichment in the list of *A. thaliana* proteins from NAC53/78
428 common interactome based on their SUBA5db annotation. Statistical significance is provided
429 through a chi-square testing.
430 (H-K) Heatmap representing the peptide enrichment (Log2FC) of the protein clusters from the
431 network Fig. 2G.
432
433 **Fig. 3. ER-Anchored Protein Sorting (ERAPS) coordinates the subcellular fate of NAC53**
434 **& NAC78.**
435 (A) Confocal microscopy pictures of GFP-NAC53/78 expressing *A. thaliana* roots. 7 dag
436 seedlings were exposed to mock treatment, BTZ 10µM, CB-5083 10µM or LS-102 100µM for
437 3h. The treatments were repeated at least three times with similar observations. Scale bars =
438 10µm
439 (B) Immunoblot against GFP on crude extracts of GFP-NAC53/78 *A. thaliana* adult plants
440 infiltrated with mock treatment, BTZ 10µM, CB-5083 10µM or LS-102 100µM for 6h. Ponceau
441 staining is used as loading control.
442 (C) Confocal microscopy pictures of *N. benthamiana* transiently co-expressing GFP-
443 NAC53/78 full-length (FL) or deleted for the transmembrane domain (ΔTM) with RFP-HRD1a
444 or RFP-HRD1b. Pearson index (ρ) indicates correlation index at the orange lines.
445 (D) Co-IP of RFP-HRD1a/b with GFP-NAC53/78. IP was performed with anti-GFP beads.
446 GFP-HDEL and free-GFP were used as negative control. The experiment was repeated twice
447 with similar results.
448 (E) Immunoblot against GFP on crude extract of *N. benthamiana* leaves transiently expressing
449 GFP-NAC53/78FL or ΔTM. Ponceau was used as loading control. Boxplots represent the
450 relative ΔTM abundance compared FL.
451 (F) *In vitro* trans-ubiquitination assays of GST-HRD1a/b against MBP-NAC53/78. Removal of
452 E1 and ATP from the reaction was used as negative control. The experiment was repeated twice
453 with similar results.
454 (G) Representation of the ER-Anchored Protein Sorting (ERAPS) mechanism. NAC53/78 are
455 ER-anchored proteins recognized and ubiquitinated by the HRD1 complex. The CDC48
456 complex subsequently extracts NAC53/78 from the ER to mediate ER-Associated Degradation
457 or allowing nuclear translocation in the context of proteasomal stress to mitigate proteotoxicity.
458
459 **Extented data Fig. 2. NAC53/78 are subjected to high level of poly-ubiquitination.**
460 (A) *In vitro* analysis of LS-102 effect on HRD1a/b ubiquitination activity. Removal of E1 and
461 ATP from the reaction was used as negative control.
462 (B) Quantification of the inhibitory effect of LS-102 (100µM) on HRD1 activity. Bar plots
463 represent the mean of three independent replicates with error bars representing the standard
464 deviation.
465 (C) Heatmaps representing the mean Log10 intensity of peptides bearing a di-glycine mark on
466 the indicated lysin residue identified by MS/MS analysis of *in vitro* trans-ubiquitination
467 reactions (see Figure 3F).
468 (D) Heatmaps representing the mean Log10 intensity of peptides bearing a di-glycine mark on
469 the indicated lysin residue identified by MS/MS analysis of IP samples generated for Figure 2.
470 (E) Alignments of NAC53 and NAC78 peptide sequence regions around the identified lysin
471 residues in panel C and D. Colors represent the residue conservation (green: conserved, shade
472 of red: not conserved). All the identified lysins in one protein are conserved in the other.
473 Underlined residues correspond to the mutated residues generated for the panel H and I.

(F) *In vitro* trans-ubiquitination assays of GST-HRD1a/b against MBP-NAC53/78 in the presence of LS-102 inhibitor. Removal of E1 and ATP from the reaction was used as negative control.
(G) Immunoblot analysis of *N. benthamiana* transiently expressing free-GFP, RFP-HDEL or dTag-NAC53/78 subjected to IP with anti-ubiquitin beads. The experiment was repeated twice with similar results.
(H) Immunoblot analysis of *N. benthamiana* transiently expressing GFP-NAC53/78 mutated for 5 lysins (Mut., see panel E) or not (WT) subjected to IP with anti- ubiquitin beads.
(I) Quantification of the relative ubiquitination levels assessed by the ratio between GFP signal and ubiquitin signal after IP as in panel H. Barplots represent the mean ratio of two replicates, normalized to the ratio of WT constructs with error bars representing the standard deviation.

Extended data Fig. 3. NAC53/78 association with CDC48 is required for their nuclear translocation.
(A) Confocal microscopy pictures of transgenic GFP-NAC53/78 root seedlings exposed to BTZ 10µM, BTZ 20µM, CB-5083 10µM or CB-5083 20µM for 3h. Scale bars = 10µm
(B) Confocal microscopy pictures of *N. benthamiana* leaves transiently co-expressing AtCDC48c-GFP with RFP-NAC53/78. Co-localization is visible in aggregate-like structures. Scale bars = 1µm
(C) Confocal microscopy representative pictures (used for panel D-E) of transgenic GFP-NAC53/78 roots treated with BTZ 10µM and CB-5083 10µM followed by Propidium Iodide staining. Scale bars = 10µm
(D-F) Boxplot representing the GFP signal quantification after confocal microscopy imaging of transgenic GFP-NAC53/78 roots exposed to BTZ 10µM or CB-5083 10µM. Black dots represent one cell. Statistical difference is assessed by a Wilcoxon-Mann-Whitney test.

Fig. 4. The transcriptional landscape of proteotoxic stress
(A) Log2FC mRNA levels of *NAC53* and *NAC78* transcripts after *Pst* infection of adult Col-0 plant leaves. The heatmap represent the mean of 4 biological replicates.
(B) Log2FC mRNA levels of 26S proteasome transcripts after *Pst* infection of Col-0 or *nac53-1 78-1* adult plant leaves. The heatmap represent the mean of 4 biological replicates. The experiment has been repeated 3 times with consistent results.
(C) Immunoblot against multiple 26S proteasome subunits on crude extracts of Col-0 or *nac53-1 78-1* adult plant leaves inoculated with *Pst* or mock solutions for 24h. Ponceau staining is used as loading control.
(D) Relative Log2FC abundance of representative 26S proteasome subunits in Col-0 or *nac53-1 78-1* adult plant leaves. The abundance is calculated relative to the mock conditions. Statistical differences are assessed via a Welch t.test (p values: n.s > 0.05, * < 0.05, ** < 0.01).
(E) Immunoblot against GFP on crude extract of *N. benthamiana* leaves transiently expressing GFP-NAC53/78 after mock treatment or *PstΔHopQ* infection for 8h. Ponceau staining is used as loading control.
(F) Immunoblot against GFP on extract of adult *A. thaliana* transgenics GFP-NAC53/78 subjected to mock treatment or *Pst* infection 8h by vacuum infiltration followed by IP with anti-GFP beads.
(G) Number of differentially expressed genes (DEGs) in the different conditions of the *nac53-1 78-1 Pst* RNAseq analysis. Total number of DEGs per condition is indicated. Colors indicate the proportion of DEGs up-regulated and down-regulated. DEGs are considered when |Log2FC| > 1.5. Genot. mock: *nac53-1 78-1* mock vs. Col-0 mock; WT *Pst*: Col-0 *Pst* vs. Col-0 mock; Mut. *Pst*: *nac53-1 78-1 Pst* vs. *nac53-1 78-1* mock; Genot. *Pst*: *nac53-1 78-1 Pst* vs. Col-0 *Pst*.
(H) Level of differential expression (Log2FC) of the 945 DEGs found in Genot. *Pst* (see panel G) for the several conditions analyzed.

525 (I) Cladogram of top 40 GO terms for BP enriched in the list of 945 DEGs. Colors represent
526 broad GO clusters.
527 (J) Venn diagram representing the overlap between the 945 DEGs and DEGs from *rpt2a-2 Pma*
528 (|Log2FC| > 0.5) or Col-0 MG132 24h (|Log2FC| > 0.5).
529 (K) Cladogram of top 30 GO terms for BP enriched in the list of 538 DEGs extracted from the
530 combined analysis (panel J). For conciseness terms are hidden and grouped in 4 processes.
531 (L) Protein network of the genes from the 945 DEGs list related to the GO BP terms from panel
532 K. Node colors refers to the 4 GO clusters from panel K.
533
534 **Extended data Fig. 4. Transcriptional analysis of proteotoxic stress reveals a trade-off**
535 **between 26S proteasome and other biological process.**
536 (A) mRNA level Log2FC of all 26S proteasome genes and associated interactors/chaperones in
537 several conditions of the *nac53-1 78-1 Pst* RNAseq.
538 (B) Number of differentially expressed genes (DEGs) in the different conditions of the *nac53-*
539 *1 78-1 Pst* RNAseq analysis. Total number of DEGs per condition is indicated. Colors indicate
540 the proportion of DEGs up-regulated and down-regulated. DEGs are considered when |Log2FC|
541 > 1.5. Genot. mock: *rpt2a-2* mock vs. Col-0 mock; WT *Pma*: Col-0 *Pma* vs. Col-0 mock; Mut.
542 *Pma*: *rpt2a-2 Pma* vs. *nac53-1 78-1* mock; Genot. *Pma*: *rpt2a-2 Pma* vs. Col-0 *Pma*.
543 (C) mRNA levels Log2FC of the 981 DEGs found in Genot. *Pma* (see panel D) for the several
544 conditions analyzed.
545 (D) mRNA level Log2FC of all 26S proteasome genes and associated interactors/chaperones in
546 the several conditions of the *rpt2a-2 Pma* RNAseq.
547 (E) Cladogram of top 40 GO terms for BP enriched in the list of 945 DEGs. Colors represent
548 the broad GO clusters.
549 (F) mRNA level Log2FC of the genes present in the 4 network modules from Figure 4L in the
550 3 Transcriptome used.
551
552 **Fig. 5. NAC53 and NAC78 coordinate the regulation of proteasome and photosynthesis**
553 **gene expression through the same cis-element.**
554 (A) Top 3 motifs found by STREME software in the promoter regions from the 4 network
555 clusters (Figure 4L). PRCE-like elements from proteasome and PhANGs clusters are
556 highlighted.
557 (B) 25bp region comprising the PRCE-like elements from LHCa3 and PSAD1 promoters used
558 in this figure. The region corresponds to the probe sequence used in panel C and D. The PRCE
559 is highlighted in red.
560 (C) Electro-Mobility Shift Assay (EMSA) of MBP-NAC53/78 with LHCa3/PSAD1 probes (see
561 panel B). As a negative control, probes were incubated without MBP-NAC53/78 (-) or with
562 MBP-NAC53/78 deleted for their DNA recognition motif (ΔRM). Experiment was repeated
563 twice with similar results.
564 (D) EMSA competition assay of MBP-NAC53/78 association with LHCa3/PSAD1 probes.
565 Competitor is applied at a concentration gradient (25X, 50X, 75X and 100X) indicated by the
566 shade of grey. WT and mutated competitors are labelled TGGGC and AAAAA, respectively.
567 Experiment was repeated twice with similar results.
568 (E) Boxplot representing association of GFP-NAC53/78 with LHCa3/PSAD1 PRCE in adult
569 *A. thaliana* transgenics lines infected with *Pst* or mock for 8h after Chromatin
570 Immunoprecipitation. The association is quantified as % of input and amplification of a region
571 in the CDS is used as negative control.
572 (F) Immunoblot against mature PhANGs proteins in Col-0 or *nac53-1 78-1* adult plant leaves
573 inoculated with *Pst* or mock solutions for 24h. Ponceau staining is used as loading control.

(G) Relative Log2FC abundance of PhANGs mature proteins immunoblotted in panel F. The abundance is calculated relative to the mock conditions. Statistical differences are assessed via a Welch t.test (p values: n.s > 0.05, * < 0.05, ** < 0.01).
(H) Photosystem II (PSII) activity measurement on Col-0 or *nac53-1 78-1* adult plants inoculated with *Pst* or mock solutions for 24h. Letters indicate the statistical group assessed by pairwise Welch t.test (p value < 0.05). The experiment was repeated 3 times with consistent results.
(I) Representative pictures of measurements from panel I. Fv/Fm values are represented by false color as indicated by the color gradient legend.
(J) Total chlorophylls and carotenoids from Col-0 or *nac53-1 78-1* adult plant leaves inoculated with *Pst* or mock solutions for 24h. Letters indicate the statistical group assessed by pairwise Wilcoxon-Mann-Whitney test (p value < 0.05). The experiment was repeated 3 times with consistent results.

Extended data Fig. 5. Characterization of the NAC53/78-PRCE module in PhANGs promoters.
(A) mRNA level Log2FC of the PhANGs clusters from Figure 4L in the 3 transcriptomes used. Genes are separated based on their associated process in the photosynthetic pathway.
(B) Mapping of the PRCE-like motifs in PhANGs promoter regions from panel A. Promoter regions are organized according to the order of the genes from panel A. Purple marks represent the position of the motifs based on their distance from the transcription starting site (TSS). The two red arrows highlight LHCa3 and PSAD1 promoter regions.
(C) Histograms representing the number of occurrences of the PRCE-like motifs across the 4 genes cluster from the network Figure 4L. Each bar represents a 20bp region, frequency *f* of promoters bearing at least one motif is indicated as a percentage.
(D) LHCa3/PSAD1 promoter activity measured by luminescence in Col-0 or *nac53-1 78-1* protoplasts extract transiently co-expressing LHCa3/PSAD1 reporter constructs and NAC53/78ΔTM. Log2FC is calculated from the luminescence level of protoplasts expressing the reporter construct alone. Replicates are a pool of at least two independent experiments. Letters indicate the statistical group assessed by pairwise Wilcoxon-Mann-Whitney test (p value < 0.05).
(E) Promoter activity as calculated in panel D for LHCa3/PSAD1 promoters deleted for their respective DNA regions from Figure 5B. Replicates are a pool of at least two independent experiments. Letters indicate the statistical group assessed by pairwise Wilcoxon-Mann-Whitney test (p value < 0.05).
(F-G) Boxplot representing the Log2FC mRNA level the indicated transcripts in Col-0, GFP-NAC53 or GFP-NAC78 seedlings treated with BTZ 10µM or mock solutions for 6h. Log2FC is calculated from Col-0 mock. Letters indicate the statistical group assessed by pairwise Wilcoxon-Mann-Whitney test (p value < 0.05).
(H) Fresh weight of seedlings from indicated genotypes grown under the indicated treatments at 10 days after germination. Letters indicate the statistical group assessed by pairwise Wilcoxon-Mann-Whitney test (p value < 0.05). Experiment was repeated 3 times with consistent results.
(I) Representative phenotypic pictures related to panel D.

Fig. 6. The proteasome autoregulatory feedback loop monitors photosynthesis homeostasis during stress responses
(A) Photosynthetic pigment content from Col-0 or *nac53-1 78-1* adult plant leaves infiltrated with Lin 200µM, BTZ 2µM or mock solutions for 24h. Content is expressed in percentage relative to Col-0 mock. Letters indicate the statistical group assessed by pairwise Wilcoxon-

Mann-Whitney test (p value < 0.05). The experiment was repeated 3 times with consistent results.
(B) Log2FC mRNA level of the indicated transcripts in Col-0, *nac53-1 78-1* adult plants leaves Lin 200µM, BTZ 2µM or mock solutions for 24h. Log2FC is calculated from Col-0 mock and *PDH1* is used as negative control. Statistical differences are assessed with a Welch t-test (p values: n.s. > 0.05, * < 0.05, ** < 0.01). The experiment was repeated twice with consistent results.
(C) Fresh weight of seedlings grown under the indicated treatments at 10-14 day after germination. The fresh weight is represented as a percentage of Col-0 mock conditions. Letters indicate the statistical groups assessed by pairwise Wilcoxon-Mann-Whitney test (p value < 0.05). Every treatment has been repeated at least twice with consistent results. Representative phenotypic pictures are included.
(D) Bacterial density shown as Log10 Colony-Forming-Unit (CFU) per leaf cm^2 in Col-0 and *hrd1a hrd1b* plants. Statistical significance is assessed by a Welch t-test (p values: * < 0.05). The experiment has been repeated three times with consistent results.
(E) Correlation heatmap of the 54 26S proteasome subunit genes and the expression of 68 PhANGs from publicly available 1223 RNAseq libraries identified in this study.

Extended data Fig. 6. The proteasome autoregulatory feedback loop transcriptional signature is a systemic response to environmental cues.
(A) PSII activity measurement on Col-0 and *nac53-1 78-1* treated as indicated in Figure 6A. Replicates are a pool of 3 independent experiments. Letters indicate the statistical group assessed by pairwise Wilcoxon-Mann-Whitney test (p value < 0.05).
(B) PSII activity measurement on Col-0 and *hrd1a hrd1b* adult plant leaves inoculated with *Pst* or mock solutions for 24h. Letters indicate the statistical group assessed by pairwise Welch t.test (p value < 0.05). The experiment was repeated 2 times with consistent results.
(C) Confocal microscopy pictures of transgenic GFP-NAC53/78 *A. thaliana* roots exposed to mock treatment, MV 100µM, GDA 100µM and Lin 100µM for 2h. The treatments were repeated at least three times with similar observations. Scale bars = 10µm
(D) Density functions of the 54 26S proteasome genes and 68 PhANGs transcripts (Log2FC) in the different transcriptome projects. Log2FC limits are -10 to +10. Treatment types and relevant condition information are provided in the figure. Plots are separated by treatment groups and subdivided by experiments.

Extended data Fig. 7. ER-anchored protein sorting (ERAPS) controls the fate of two proteasome activators for intracellular organelle communication during proteotoxic stress.
In steady state conditions, the ER-anchored protein sorting system (ERAPS) promotes the constitutive degradation of NAC53/78 via the 26S proteasome. Meanwhile, PhANGs expression is activated and subsequent chloroplastic import permits the maintenance of active photosynthesis. Upon proteotoxic stress, the chloroplast import machinery is targeted for proteasomal degradation. This leads to an accumulation of PhANGs precursors which are therefore subjected to proteasomal degradation, inducing proteotoxicity. Thus, to avoid proteotoxicity, the ERAPS system facilitates the nuclear translocation of NAC53/78, to activate the production of a new proteasome complex and to repress PhANGs expression to mitigate substrate accumulation.

673 # Methods

674 **Plant materials and growth conditions**

675 *A. thaliana* Columbia-0 (Col-0) ecotype was considered as WT. T-DNA insertion mutants for
676 *NAC53* (nac53-1, SALK_009578C) and *NAC78* (nac78-1, SALK_025098) were previously
677 described in Gladman et al., 2016. T-DNA insertion mutants for *RPT2a* was previously
678 described[20]. T-DNA insertion mutants for *HRD1a (hrd1a*, SALK_032914) and *HRD1b* (*hrd1b,*
679 SALK_061776) were obtained from Yasin Dagdas. *promUBQ10*::GFP-NAC53 and
680 *promUBQ10*::GFP-NAC78 transgenics lines were obtained by *Agrobacetrium tumefaciens*
681 floral dipping of Col-0 plants. For experiments on seedlings, seeds were surface sterilized
682 10min with 1.3% sodium hypochlorite. Seeds were sown on ½ Murashige and Skoog (MS)
683 medium plus 1% sucrose and stratified for 2 days. Plants were grown under long day conditions
684 (light/dark cycles: 16h 22°C/8h 20°C, 130µmol.mm².s^{-1} light intensity, 70% relative humidity).
685 For experiments on adult plants, plants were grown under short day conditions (light/dark
686 cycles: 12h 22°C/ 12h 20°C, 90µmol.mm².s^{-1} light intensity, 70% relative humidity). Plants
687 were grown 4-5 weeks until use.

688

689 ***Nicotiana benthamiana* growth**

690 *N. benthamiana* plants were grown under long day conditions (light/dark cycles: 16h/8h, at
691 21°C and 70% humidity) and typically used 4 weeks after germination for confocal microscopy
692 experiments and 5 weeks after germination for co-immunoprecipitation experiments.

693

694 **Bacterial strains**

695 *For Pseudomonas syringae* pv. *tomato* DC3000 wild-type and *Pseudomonas syringae* pv.
696 *maculicola* strains ES4326 were grown on King's B medium containing rifampicin 100µg.mL^{-}
697 ^{1} at 28°C. For floral dipping and transient expression in *Nicotiana benthamiana* leaves,
698 *Agrobacterium tumefaciens* C58C1 strain was grown in LB broth high salt (Duchefa L1704)
699 containing the required antibiotics at 28°C. For molecular cloning, *Escherichia coli* Top10
700 strain was grown in LB broth high salt (Duchefa L1704) containing the required antibiotics at
701 37°C. For protein purification, *Escherichia coli* BL21 (DE3) was grown in LB broth high salt
702 (Duchefa L1704) containing the required antibiotics at 37°C or 16°C.

703

704 **Gene Accession**

705 Arabidopsis genome initiative (AGI) locus identifier of the principal genes investigated in this
706 study are the following: *NAC53* (AT3G10500), *NAC78* (AT5G04410), *HRD1a* (AT3G16090),

707 *HRD1b* (AT1G65040), *CDC48c* (AT5G03340), *RPT2a* (AT4G29040), *LHCa3* (AT1G61520),
708 *PSAD1* (AT4G02770).
709
710 **Molecular cloning**
711 For chimeric protein constructs generated in this study, protein coding sequence (CDS) of the
712 desired genes were amplified from *A. thaliana* cDNA. For Golden Gate based cloning[41], CDS
713 were amplified with addition of flanking regions including BpiI/BsaI sites and final constructs
714 were generated using the LI CDS module of interest and desired other modules and assembled
715 in the LIIa F 1-2 vector. For GATEWAY™ based cloning, CDS were amplified with addition
716 of attb1/attb2 flanking regions and final constructs were generated through BP clonase™ II
717 enzymatic reaction and LR Clonase™ II enzymatic reaction into the desired destination vectors.
718 All LI and GATEWAY™ entry clones were verified by sanger sequencing.
719
720 **Seedlings phenotyping**
721 For phenotyping assay, seeds were sown on ½ MS 1% sucrose round petri dish supplemented
722 with the indicated concentration of drug or a mock treatment. After 10 to 14 days of growth
723 fresh weight was measured. For one replicate, 5 representative seedlings were scaled together
724 on an analytical scale (resolution 0.0001g). Typically, 5 replicates were measured for
725 subsequent statistical analyses.
726
727 **Transient expression in *N. benthamiana* leaves**
728 Bacterial suspension was centrifuged for 4min at 4000g after overnight incubation of *A.*
729 *tumefaciens* strain carrying the desired expression construct. Supernatant was removed and
730 pellet was resuspended in 500µl of agroinfiltration buffer (10mM $MgCl_2$, 10mM MES pH 5.7).
731 OD600 was measured and infiltration solutions were diluted to reach final 0.5 OD600 in
732 agroinfiltration buffer supplemented with 200µM acetoseryringone. Solution were incubated in
733 dark at least 1h prior to infiltration. Infiltrated tissues were used 30h post infiltration for
734 subsequent experimental procedures.
735
736 **Protein purification**
737 Recombinant proteins were expressed in E. coli BL21(DE3) by IPTG induction. Bacterial
738 solution was centrifuged 20min at max speed and pellet was subjected to sonication after
739 resuspension in 1mL MBP-buffer (20 mM TRIS-HCl pH 7.5, 200mM NaC, 1mM EDTA) or
740 1mL IPP50 (10 mM Tris-HCl, pH 8.0. 150mM NaCl, 0.1% NP40). Sonicated samples were

741 used for purification by affinity chromatography using amylose resin (New England Biolabs)
742 for MBP-NAC53/78 or glutathione sepharose 4B (cytiva) for GST-HRD1a/b. For recombinant
743 His-UBA1 and His-UBC8 protein were purified using Ni-Ted resin (Macherey-Nagel).
744
745 ***In vitro* ubiquitination assay**
746 In vitro ubiquitination assay was performed as described previously[42]. Samples were separated
747 by SDS–PAGE electrophoresis using 4–15% Mini-PROTEAN® TGX™ Precast Protein Gels
748 (BioRad) followed by detection of the ubiquitinated substrate by immunoblotting using anti-
749 MBP (New England Biolabs), anti-GST and anti-ubiquitin (Santa Cruz Biotechnology)
750 antibodies.
751
752 **Co-immunoprecipitation**
753 Plant tissue was homogenized in a mortar with liquid nitrogen to keep the sample frozen during
754 the process. And extracted in 1ml/g of extraction buffer (10% glycerol, 25 mM Tris pH 7.5, 1
755 mM EDTA, 150 mM NaCl, 1 mM DTT, 0.5% Triton X, 1X protease cocktail inhibitor (Sigma)).
756 Solution was vortexed for 3min and incubated in cold room on rotator for 10min following a
757 30min centrifugation at 4000g, 4°C. Supernatant was filtered. 50µl of filtrate was sampled as
758 input, supplemented with 12.5µL laemmli buffer 4X (Biorad) and boiled for 10min at 95°C.
759 Next, 10µl/g of ChromoTek GFP-Trap® or RFP-Trap Agarose beads were added and tubes
760 were incubated 2-3h in cold room. Tubes were then centrifuge at 800g for 1min; supernatant
761 was carefully removed and pelleted beads were transferred to 1.5mL microcentrifuge tube in
762 1mL of washing buffer (10% glycerol, 25 mM Tris pH 7.5, 1 mM EDTA, 150 mM NaCl, 0.5%
763 Triton X-100, 1X protease cocktail inhibitor (Sigma)). Washing was performed by
764 centrifugation at 800g for 1min using 1mL washing buffer. After last washing, Laemmli buffer
765 2X (Biorad) was added to equal amounts of beads and sample was boiled 10min at 95°C.
766
767 **RNA isolation & RT-qPCR**
768 Total RNA isolation was performed using RNeasy Plant Mini Kit (Qiagen 74904) according to
769 manufacturer instructions. To exclude potential contaminant DNA, RNA samples were
770 subjected to DNase I treatment (Thermo scientific™) following provider instructions. For RNA
771 sequencing, integrity and RNA concentration was determined (2100 Bioanalyzer, Agilent). For
772 RT-qPCR sample analysis was performed as described previously[43]; cDNA synthesis was
773 performed using LunaScript® RT SuperMix Kit (NEB) following provider recommendation.
774 qPCR was performed using MESA BLUE qPCR 2X MasterMix Plus for SYBR®

775 Assay (Eurogentec) using a 2-step reaction protocol for 40cycles with systematic evaluation of
776 primer melting curve. mRNA level was quantified based on the ΔΔCt method followed by Log2
777 transformation.
778
779 **NanoLC-MS/MS analysis and data processing**
780 For purification, proteins were subjected to a NuPAGE 12% gel (Invitrogen) and in-gel trypsin
781 digestion was done on Coomassie-stained gel pieces with a modification: *chloroacetamide* was
782 used instead of iodoacetamide for carbamidomethylation of cysteine residues to avoid
783 formation of lysine modifications isobaric to two glycine residues left on ubiquitinylated lysine
784 after tryptic digestion. Next, peptides mixture were desalted using C18 Stage tips and run on an
785 Easy-nLC 1200 system coupled to a Q Exactive HF mass spectrometer (both Thermo Fisher
786 Scientific) as described elsewhere[44] with some modifications: separation of the peptide
787 mixtures was done using a 87-min or 127-min segmented gradient from 10-33-50-90% of
788 HPLC solvent B (80% acetonitrile in 0.1% formic acid) in HPLC solvent A (0.1% formic acid)
789 at a flow rate of 200 nl/min. The seven most intense precursor ions were sequentially
790 fragmented in each scan cycle using higher energy collisional dissociation (HCD)
791 fragmentation. In all measurements, sequenced precursor masses were excluded from further
792 selection for 30 s. The target values were 10^5 charges for MS/MS fragmentation and 3×10^6
793 charges for the MS scan.
794 Acquired MS spectra were processed with MaxQuant software package version 1.5.2.8 with an
795 integrated Andromeda search engine. For *in vivo* IP samples, database search was performed
796 against a *N. benthamiana* database containing 74,802 protein entries[45], the sequences of eGFP-
797 NAC53/78, mCerrulean3-NAC53/78-mCherry and 285 commonly observed contaminants.
798 For *in vitro* ubiquitination samples, database search was performed against a Uniprot *E. coli*
799 database (4,403 entries, downloaded on 7th of October 2020), the sequences of MBP-
800 NAC53/78, GST-HRD1a/b and 285 commonly observed contaminants.
801 Endoprotease trypsin was defined as a protease with a maximum of two missed cleavages.
802 Oxidation of methionine, phosphorylation of serine, threonine, and tyrosine, GlyGly dipeptide
803 on lysine residues, and N-terminal acetylation were specified as variable modifications.
804 Carbamidomethylation on cysteine was set as a fixed modification. Initial maximum allowed
805 mass tolerance was set to 4.5 parts per million (ppm) for precursor ions and 20 ppm for fragment
806 ions. Peptide, protein, and modification site identifications were reported at a false discovery
807 rate (FDR) of 0.01, estimated by the target-decoy approach (Elias and Gygi). The iBAQ

808 (Intensity Based Absolute Quantification) and LFQ (Label-Free Quantification) algorithms
809 were enabled, as was the "match between runs" option[46].
810
811 **Photosynthesis monitoring**
812 For photosynthetic pigment concentration, 2 leaf discs (6mm) were sampled and incubated
813 over-night in 1mL acetone 100% on a rotating wheel in cold room. Tubes were next centrifuged
814 for 3min at 400g. 200µl of was then pipetted in a transparent 96-well plate and absorbance was
815 measured at 470nm, 646nm and 663nm using a plate reader (Tecan Infinite 200 PRO®).
816 Acetone 100% was used as blank. Concentration was calculated as following the obtained from
817 Karlsruher Institut für Technologie (KIT, https://www.jkip.kit.edu/molbio/998.php,
818 "Chlorophyll and Carotenoid determination in leaves"). Values were then then expressed as
819 ng.mm².For photosynthetic efficiency, photosystem II (PSII) activity was measured by
820 quantifying the maximum photosystem II yield, Fv/Fm via the saturation pulse methods on dark
821 acclimated plants (Schreiber 2004), a Imaging-PAM chlorophyll fluorometers: Maxi version
822 v2-46i, for measurements or Dual-PAM100 (Walz GmbH, Effeltrich, Germany).
823
824 **Bacterial Infection**
825 *Pst* overnight liquid culture was centrifuged for 15min at 4000g. Bacterial pellet was
826 resuspended in 5mL of $MgCl_2$ 10mM prior to OD600 measurement.
827 For qPCR, RNAseq and western blot analysis; a *Pst* solution at OD600=0.2 in 10mM $MgCl_2$
828 was used. Adult plant leaves were syringe infiltrated with the *Pst* solution or a 10mM $MgCl_2$
829 solution for 24h until sampling. For IP and Chromatin-IP on *A. thaliana*, *Pst* infiltration was
830 prepared as explained above and detached whole rosettes of adult plants were vacuum
831 infiltrated 2 times 2 min at < 15mbar. For mock, control solution (10mM $MgCl_2$) was used
832 similarly. Rosettes were put back in the growth chamber for 8h on multiple layers of wet tissue.
833 For assessment of bacterial density, *Pst* infiltration solution was prepared in 10mM $MgCl_2$ at
834 an OD600 of 0.0001. Adult plant leaves were syringe infiltrated with the *Pst* infiltration solution
835 for 72h in high humidity conditions. Next, 2 leaf disks per replicates were sampled and
836 homogenized in 200µl 10mM $MgCl_2$ and a serial dilution from 10^{-1} to 10^{-6} in 200µL was done.
837 For bacterial counting, 20µL of 10^{-5} and 10^{-6} dilutions were plated. Growing colony-forming
838 units were counted and Log10CFU/cm² was calculated.
839
840 **Chromatin Immuno-Precipitation**

841 For Chromatin-IP, after Arabidopsis rosettes were vacuum infiltrated for 30min with a fixation
842 buffer solution (1% formaldehyde, 10mM KH2PO4 pH 7, 50mM NaCl, 0.1M sucrose, 0.01%
843 Triton X-100). Plant material (1g) was dried and frozen in liquid nitrogen. Tissue was ground
844 in 5mL nuclei isolation buffer (20mM Hepes pH8, 250mM sucrose, 1 mM $MgCl_2$, 5mM KCl,
845 40% Glycerol, 0.25% Triton X-100, 0.1mM PMSF, 0.1% 2-mercaptoethanol, 1µM BTZ). The
846 solution was filtered and subjected to 10min centrifugation at 4°C, 3000g. Pellet was
847 resuspended in 1mL nuclei isolation buffer and centrifuged 5min, at 4°C, 3000g, two. Pellet
848 was resuspended in 200µl M3 buffer (10mM KH2PO4 pH7, 0.1mM NaCl, 10mM 2-
849 mercaptoethanol) and centrifuged 5min, 4°C, 3000g. Nuclei pellet was resuspended in 1mL
850 sonication buffer (10mM KH2PO4 pH7, 0.1mM NaCl, 0.5% Sarkosyl, 10mM EDTA).
851 Sonication was performed with an Active Motif Sonicator (Amp 25%; Pulse: 30sec ON – 30sec
852 OFF; Timer: 300sec). Sonicated sample was centrifuged for 5min, 4°C at max speed.
853 Supernatant was tranferred to a new 1 tube and 10% (v/v) Triton X-100 was added to neutralize
854 the sarkosyl. 5% (v/v) of this solution was saved as input sample. For IP, 15µL ChromoTek
855 GFP-Trap® were activates in 15µL IP buffer (50mM Hepes pH 7.5, 150mM NaCl, 5mM
856 $MgCl_2$, 10uM ZnSO4, 1% Triton X -100, 0.05% SDS), added to the tube and incubated 3h on
857 a rotating wheel at 4°C. Beads were washed 4 times by centrifuging for 30sec, at 1000g and
858 subsequent incubation on rotating wheel in 500µL buffer for 3 min; twice in IP buffer, once in
859 LNDET buffer (0.25 LiCl, 1% NP-40, 1% deoxycholate, 1mM EDTA pH 8, 10mM Tris pH 8)
860 and once in TE buffer (10mM Tris pH 8, 1mM EDTA pH 8). After the last washing step, beads
861 were centrifuged for 30sec at 1000g, resuspended in 200µL EB buffer (50mM Tris pH 8, 10mM
862 EDTA pH 8, 1% SDS) supplemented with 8µL 5M NaCl to reverse cross-linking and incubated
863 at 65°C for at least 6h. At this step input sample was added and treated similarly. For protein
864 digestion, 1µL of Proteinase K (Thermo Scientific) was added and incubated for 1h at 45°C.
865 Finally, DNA was purified.
866 For DNA quantification, qPCR was performed using MESA BLUE qPCR 2X MasterMix Plus
867 for SYBR® Assay (Eurogentec) in technical triplicates. For quantification, % of input was
868 calculated.
869
870 **Immunoblot analysis**
871 For immunoblot analysis, sample processing was performed as described previously[43].
872
873 **Electromobility Shift Assay**

874 For EMSA assays, complementary DNA oligos were synthesized by EuroFins Genomics with
875 ATTO565 dye linked to the 5' end of minus strand for probes. To generate double stranded
876 probes, complementary oligos were incubated at 2µM in annealing buffer (25mM HEPES-
877 KOH pH 7.8, 40mM KCl) at 70°C for 5min and cool down to room temperature.
878 EMSA reactions were performed in 20µL reaction buffer (25 mM HEPES-KOH pH 7.8, 40
879 mM KCl, 1 mM DTT, 10% Glycerol) using 1µg purified MBP-NAC53/78 and 50ng DNA probe
880 for 30min at 25°C. Reactions were subjected to native polyacrylamide migration with TGX
881 FastCast 7.5% Acrylamide gels (Biorad) in TAE (Tris-base 40 mM pH 8.3, 20mM acetic acid,
882 1mM EDTA). After migration, probes were imaged using a Typhoon FLA 9000 Gel Scanner.
883
884 **Luciferase reporter assay in Protoplasts**
885 For promoter activity analysis, *Arabidopsis* mesophyll protoplasts were generated as described
886 perviously[27]. Luciferase quantification was performed according to Dual-Luciferase® Reporter
887 Assay System from Promega recommendation (see link).
888

889 ## Data analysis

890 For all statistical analysis, R programming language was used in the Rstudio environment. For
891 non-omics data, the statistical test and associated p value threshold for each analysis are
892 indicated in the figure legends. Data dispersion, medians and quantiles are represented with
893 boxplots and replicates displayed in every figures. For bar plots in Extended Data Fig. 2,
894 number of replicates are indicated in the figure legend, error bars represent the standard
895 deviation from the mean.
896
897 **RNA sequencing**
898 For *rpt2a-2 Pma* transcriptome, sequencing was performed by ATLAS Biolabs, Berlin. For
899 *nac53-1 78-1 Pst* transcriptome, sequencing was performed by the NGS Competence Center,
900 Tübingen. After quality control, reads were mapped to the *A. thaliana* TAIR10 reference
901 genome. The mapped reads were counted with *htseq-count* for subsequent analysis. Log2FC
902 and false discovery rate (FDR) were determined using R package DEseq2[47] with default
903 settings. A gene is considered significantly differentially expressed when its FDR < 0.05.
904 Log2FC threshold is indicated in the figure legends according to the analysis.
905
906 **IP-MS/MS analysis**

907 For IP-MS/MS analysis, Log2FC and false discovery rate (FDR) for each protein group were
908 determined as described previously[42]. For downstream analysis, to each protein group a unique
909 Agi-code was assigned by blasting every *N. benthamiana* protein present in the protein group
910 against *A. thaliana* proteome and taking the most frequent Agi-code with the best E-value. An
911 E-value threshold of e-10 was used, in case of absence of *A. thaliana* the protein group was not
912 considered for downstream analysis. For heatmap representation, in case multiple protein
913 groups correspond to the same *A. thaliana* orthologs the mean Log2FC is represented.
914
915 **Meta-Transcriptomic analysis**
916 For meta-transcriptomic analysis in Fig. 6 and Extended data Fig. 6, fragments per kilobase per
917 million counts were retrieved from the data base (http://ipf.sustech.edu.cn/pub/athrna/).
918 Log2FC for individual genes in every project was calculated based on the control RNAseq
919 libraries as annotated in the original publication[31]. Filtering of relevant projects for subsequent
920 correlation analysis was done based on the median |Log2FC|. Median|Log2FC| > 0.5 was used
921 for identification of projects with at least one gene cluster transcriptionally impacted and
922 median |Log2FC| > 0.3219 was used for identification of projects in which 26S proteasome and
923 PhANGs clusters were co-transcriptionally impacted. Pearson correlations were calculated.
924 Only correlations with p-value < 0.05 were considered significant and used for calculation of
925 mean/median.
926
927 **Omics downstream analysis: Gene ontology, Protein Network, subcellular enrichment &**
928 **cis-element analysis**
929 For Gene Ontology enrichment, the list of Agi-code was uploaded into ShinyGO software
930 (http://bioinformatics.sdstate.edu/go/). Cladogram of the indicated number of top terms for the
931 indicated type of terms was used for graphical representation. Table of annotations was
932 extracted for further analysis.
933 For network creation, list of Agi-code was provided to the string database (https://string-
934 db.org/). Table of interactions was extracted and uploaded to cytoscape software
935 (https://cytoscape.org/) for network generation, design, and annotation. For purposes of clarity,
936 network nodes were manually arranged. Edge transparency relate to the strength of interaction
937 with opaque edges corresponding to strong interactions and transparent edges to weak
938 interactions. Node color corresponds to manual annotation inferred based on GO annotations
939 and further curated from the literature.

940 For subcellular compartment enrichment, the list of Agi-code was uploaded into SUBA5db
941 (https://suba.live/). Compartment annotation was extracted, and occurrence of every
942 compartment was counted to estimate the list distribution. For theorical distribution 20 Agi-
943 code lists of the same length were randomly generated and processed similarly. The mean
944 distribution of the 20 lists was used as theorical distribution. Enrichment for every compartment
945 was calculated as a Log2FC of the ratio between the observed proportion and the theorical one.
946
947 **Cis-Regulatory Element analysis**
948 For cis-regulatory element analysis, promoter sequences of 1000bp upstream of the
949 transcription starting site were retrieved from plant ensembl database using biomart browser
950 (https://plants.ensembl.org/biomart/). For identification of novel cis-regulatory elements in
951 Figure 5A, promoter sequences of the several gene clusters were analyzed using the STREME
952 software (https://meme-suite.org/meme/tools/streme) with default settings. For mapping and
953 counting, promoter sequences were analyzed in R.
954
955 **Immunoblot semi-quantitative analysis**
956 Raw image of the immublot signals against the protein of interest and the corresponding loading
957 control were processed using Fiji software (https://imagej.net/software/fiji/downloads). Image
958 was converted to 8-bit format, background was subtracted. Individual lanes were quantified by
959 measurement of the peak area after circumscription with the rectangular ROI selection and
960 "Gels" function. The obtained values for individual bands were normalized by the
961 corresponding loading control values. Log2FC was calculated using the corresponding mock
962 sample of the same genotype.
963
964 **Confocal microscopy imaging**
965 Confocal microscopy was done using an inverted Zeiss LSM 880 microscope, an upright Leica
966 SP8 microscope or an inverted Leica Stellaris 8 microscope. For mCerrulean3 imaging,
967 excitation = 458nm and emission window = 465nm-500nm; for eGFP or sGFP imaging,
968 excitation = 488nm and emission window = 510nm-540nm; for mRFP or mCherry imaging,
969 excitation = 561nm and emission window = 590nm- 630nm; in addition, chlorophyll auto
970 fluorescence was vizualized in the far-red wavelength. Images were acquired with a 40X water
971 immersion objective, pinhole set to 1 airy unit, resolution of acquisition >1024x1024 with a
972 line average of 4.

After acquisition images were processed in Fiji Software. For images obtained from Leica microsystem devices, a gaussian blur (radius 0.75) was applied. For clarity purposes, contrast on the individual channels was manually adjusted.

For subcellular quantification of GFP signal, all images used were acquired on the Zeiss LSM 880 with a 16bits depth. Prior to imaging seedlings were incubated for 10min in a 10µM propidium iodide (PI) ½ MS solution followed by a brief washing in clear ½ MS. For PI fluorescence, was excitation = 488nm and emission window = 590nm-660nm. Each cell and corresponding nucleus were segmented using the polygon ROI selection tool in Fiji software. Signal proportion in the nucleus was quantified by dividing integrated density of nucleus ROI by integrated density of whole cell ROI and ratio of signal between nucleus and cytosol was calculated dividing nucleus ROI mean intensity by cytosolic ROI mean intensity.

For calculation of co-localization index the image J plugin "co-localization finder" was used to calculate pearson index or plot profile of GFP and RFP signals was extracted at the indicated line using Fiji software and the pearson index was calculated between the two profiles.

RESOURCE AVALAIBILITY

Source code of R and Python3 scripts used for the several computational analysis done in this study will be put available on https://github.com/Gogz31 or can be directly requested.

DATA AVAILABILITY

The mass spectrometry data from this publication will be made available on the PRIDE archive (https://www.ebi.ac.uk/pride/archive/) and with the identifier (PXDXXXXX; and (PXDXXXX). All relevant proteomics data are made available in the supplemental information.

Acknowledgements

We thank Yasin Dagdas and Marja Timmermans for critical discussions during the thesis advisory committee meeting. We are thankful to #theustunlab members Ophélie Léger, Paul Gouguet for stimulating discussions and Manuel González Fuente for editorial issues. We thank Nan Wang for technical advice on the Ch-IP procedure, Robert Morbitzer for technical support on the golden gate molecular cloning. We are grateful to Ana Gabriela Andrade-Galan and Lars Pospisil for technical support on the Photosystem II activity measurement. Stefan Bieker for the help with the computational analysis. We thank Silke Wahl, Anke Biedermann and Irina Droste-Borel for their technical support in sample preparation for MS. We are thankful to Jos Schippers, Yasin Dagdas and Richard Vierstra for sharing published material. This work was

supported by an Emmy Noether Fellowship GZ: UE188/2-1 from the Deutsche Forschungsgemeinschaft (DFG; to S.Ü.) and through the collaborative research council 1101 (SFB1101; to G.L.). We thank the confocal microscopy facility of ZMBP that is supported by funds from DFG (INST 37/819-1 FUGG and INST 37/965-1 FUGG) and the confocal microscopy facility of RUB (DFG Project number 523980288, GZ:INST 213/1180-1 FUGG).

Author Contribution

S.Ü. conceived the project. G.L. performed most experiments, analyzed the data, and performed all computational analysis. M.R. performed the *in vitro* ubiquitination assays. D.B performed the EMSA, assisted with the Luciferase reporter assay and the molecular cloning. D.S. generated the *rpt2a-2 Pma* transcriptome under the supervision of F.B..M.F.W and B.M. performed LC-MS/MS analysis. S.Ü. wrote the manuscript together with G.L..

References

1. Jayaraj, G. G., Hipp, M. S. & Ulrich Hartl, F. Functional modules of the proteostasis network. *Cold Spring Harb Perspect Biol* **12**, (2020).
2. Orosa, B. *et al.* Plant proteostasis – shaping the proteome: a research community aiming to understand molecular mechanisms that control protein abundance. *New Phytologist* **227**, 1028–1033 (2020).
3. Langin, G., González-Fuente, M. & Üstün, S. The Plant Ubiquitin – Proteasome System as a Target for Microbial Manipulation. 1–25 (2023).
4. Langin, G., Gouguet, P. & Üstün, S. Microbial Effector Proteins – A Journey through the Proteolytic Landscape. *Trends Microbiol* **xx**, 1–13 (2020).
5. Raffeiner, M., Zhu, S., González-Fuente, M. & Üstün, S. Interplay between autophagy and proteasome during protein turnover. *Trends Plant Sci* **28**, 698–714 (2023).
6. Marshall, R. S. & Vierstra, R. D. Dynamic Regulation of the 26S Proteasome : From Synthesis to Degradation. **6**, (2019).
7. Nguyen, H. M. *et al.* An upstream regulator of the 26S proteasome modulates organ size in Arabidopsis thaliana. *Plant Journal* **74**, 25–36 (2013).
8. Gladman, N. P., Marshall, R. S., Lee, K.-H. & Vierstra, R. D. The Proteasome Stress Regulon Is Controlled by a Pair of NAC Transcription Factors in Arabidopsis. *Plant Cell* **28**, 1279–1296 (2016).
9. Langin, G., González-fuente, M. & Üstün, S. The Plant Ubiquitin – Proteasome System as a Target for Microbial Manipulation. 1–25 (2023).
10. Wang, X., Xu, H., Ju, D. & Xie, Y. Disruption of Rpn4-induced proteasome expression in Saccharomyces cerevisiae reduces cell viability under stressed conditions. *Genetics* **180**, 1945–1953 (2008).
11. Ma, M. & Liu, Z. L. Comparative transcriptome profiling analyses during the lag phase uncover YAP1, PDR1, PDR3, RPN4, and HSF1 as key regulatory genes in genomic adaptation to the. *BMC Genomics* 12–14 (2010).
12. Christianson, J. C. & Carvalho, P. Order through destruction : how ER-associated protein degradation contributes to organelle homeostasis. **44**, 1–15 (2022).

13. Fonseca, D. & Carvalho, P. EGAD ! There is an ERAD doppelganger in the Golgi . *EMBO J* **38**, 1–3 (2019).
14. Liao, P. C., Wolken, D. M. A., Serrano, E., Srivastava, P. & Pon, L. A. Mitochondria-Associated Degradation Pathway (MAD) Function beyond the Outer Membrane. *Cell Rep* **32**, 107902 (2020).
15. Ling, Q. *et al.* Ubiquitin-dependent chloroplast-associated protein degradation in plants. **4467**, (2019).
16. Li, J. *et al.* The CDC48 complex mediates ubiquitin-dependent degradation of intra-chloroplast proteins in plants. *Cell Rep* **39**, 110664 (2022).
17. Hristou, A., Grimmer, J. & Baginsky, S. The Secret Life of Chloroplast Precursor Proteins in the Cytosol. *Mol Plant* **13**, 1111–1113 (2020).
18. Bragoszewski, P., Turek, M. & Chacinska, A. Control of mitochondrial biogenesis and function by the ubiquitin - Proteasome system. *Open Biol* **7**, (2017).
19. Krämer, L., Groh, C. & Herrmann, J. M. The proteasome: friend and foe of mitochondrial biogenesis. *FEBS Lett* **595**, 1223–1238 (2021).
20. Üstün, S. *et al.* The Proteasome Acts as a Hub for Plant Immunity and Is Targeted by Pseudomonas Type III Effectors. *Plant Physiol* **172**, 1941–1958 (2016).
21. Üstün, S. *et al.* Bacteria Exploit Autophagy for Proteasome Degradation and Enhanced Virulence in Plants. *Plant Cell* (2018).
22. Marshall, R. S. *et al.* ATG8-Binding UIM Proteins Define a New Class of Autophagy Adaptors and Receptors Article ATG8-Binding UIM Proteins Define a New Class of Autophagy Adaptors and Receptors. *Cell* 1–16 (2019) doi:10.1016/j.cell.2019.02.009.
23. Wu, G. Z. *et al.* Control of retrograde signalling by protein import and cytosolic folding stress. *Nat Plants* **5**, 525–538 (2019).
24. Yagishita, N. *et al.* RING-finger type E3 ubiquitin ligase inhibitors as novel candidates for the treatment of rheumatoid arthritis. *Int J Mol Med* **30**, 1281–1286 (2012).
25. Littlejohn, G. R., Breen, S., Smirnoff, N. & Grant, M. Chloroplast immunity illuminated. *New Phytologist* **229**, 3088–3107 (2021).
26. Leister, D. & Schneider, A. From Genes to Photosynthesis in Arabidopsis thaliana. *Int Rev Cytol* **228**, 31–83 (2003).
27. Yoo, S.-D., Cho, Y.-H. & Sheen, J. Arabidopsis mesophyll protoplasts: a versatile cell system for transient gene expression analysis. *Nat Protoc* **2**, 1565–72 (2007).
28. Grimmer, J. *et al.* Mild proteasomal stress improves photosynthetic performance in Arabidopsis chloroplasts. *Nat Commun* 1–11 doi:10.1038/s41467-020-15539-8.
29. Stephani, M. *et al.* A cross-kingdom conserved er-phagy receptor maintains endoplasmic reticulum homeostasis during stress. *Elife* **9**, 1–105 (2020).
30. Chen, Q. *et al.* HRD1-mediated ERAD tuning of ER-bound E2 is conserved between plants and mammals. *Nat Plants* **2**, 1–7 (2016).
31. Zhang, H. *et al.* A Comprehensive Online Database for Exploring ∼20,000 Public Arabidopsis RNA-Seq Libraries. *Mol Plant* **13**, 1231–1233 (2020).
32. Woodson, J. D. & Chory, J. Organelle signaling: How stressed chloroplasts communicate with the nucleus. *Current Biology* **22**, R690–R692 (2012).
33. Richter, A. S. *et al.* Retrograde signaling in plants: A critical review focusing on the GUN pathway and beyond. *Plant Commun* **4**, (2023).
34. Waters, M. T. *et al.* GLK transcription factors coordinate expression of the photosynthetic apparatus in Arabidopsis. *Plant Cell* **21**, 1109–1128 (2009).
35. Kacprzak, S. M. *et al.* Plastid-to-nucleus retrograde signalling during chloroplast biogenesis does not require ABI4. *Plant Physiol* **179**, 18–23 (2019).
36. Sun, X. *et al.* A chloroplast envelope-bound PHD transcription factor mediates chloroplast signals to the nucleus. *Nat Commun* **2**, (2011).

37. Page, M. T. *et al.* Seedlings lacking the PTM protein do not show a genomes uncoupled (Gun) mutant phenotype. *Plant Physiol* **174**, 21–26 (2017).
38. Koussevitzky, S. *et al.* Signals from Chloroplasts Converge to Regulate Nuclear Gene Expression. *Science (1979)* **316**, 715–719 (2007).
39. Tokumaru, M. *et al.* Ubiquitin-proteasome dependent regulation of the GOLDEN2-LIKE 1 transcription factor in response to plastid signals. *Plant Physiol* **173**, 524–535 (2017).
40. Lehrbach, N. J. & Ruvkun, G. Proteasome dysfunction triggers activation of SKN-1A/Nrf1 by the aspartic protease DDI-1. *Elife* **5**, 1–19 (2016).
41. Binder, A. *et al.* A modular plasmid assembly kit for multigene expression, gene silencing and silencing rescue in plants. *PLoS One* **9**, (2014).
42. Leong, J. X. *et al.* A bacterial effector counteracts host autophagy by promoting degradation of an autophagy component. 1–17 (2022) doi:10.15252/embj.2021110352.
43. Langin, G. & Üstün, S. A Pipeline to Monitor Proteasome Homeostasis in Plants. in *Plant Proteostasis: Methods and Protocols* (eds. Lois, L. M. & Trujillo, M.) 351–363 (Springer US, New York, NY, 2023). doi:10.1007/978-1-0716-2784-6_25.
44. Kliza, K. *et al.* Internally tagged ubiquitin: A tool to identify linear polyubiquitin-modified proteins by mass spectrometry. *Nat Methods* **14**, 504–512 (2017).
45. Kourelis, J. *et al.* A homology-guided, genome-based proteome for improved proteomics in the alloploid Nicotiana benthamiana. *BMC Genomics* **20**, 1–15 (2019).
46. Schwanhüusser, B. *et al.* Global quantification of mammalian gene expression control. *Nature* **473**, 337–342 (2011).
47. Love, M. I., Huber, W. & Anders, S. Moderated estimation of fold change and dispersion for RNA-seq data with DESeq2. *Genome Biol* **15**, 1–21 (2014).

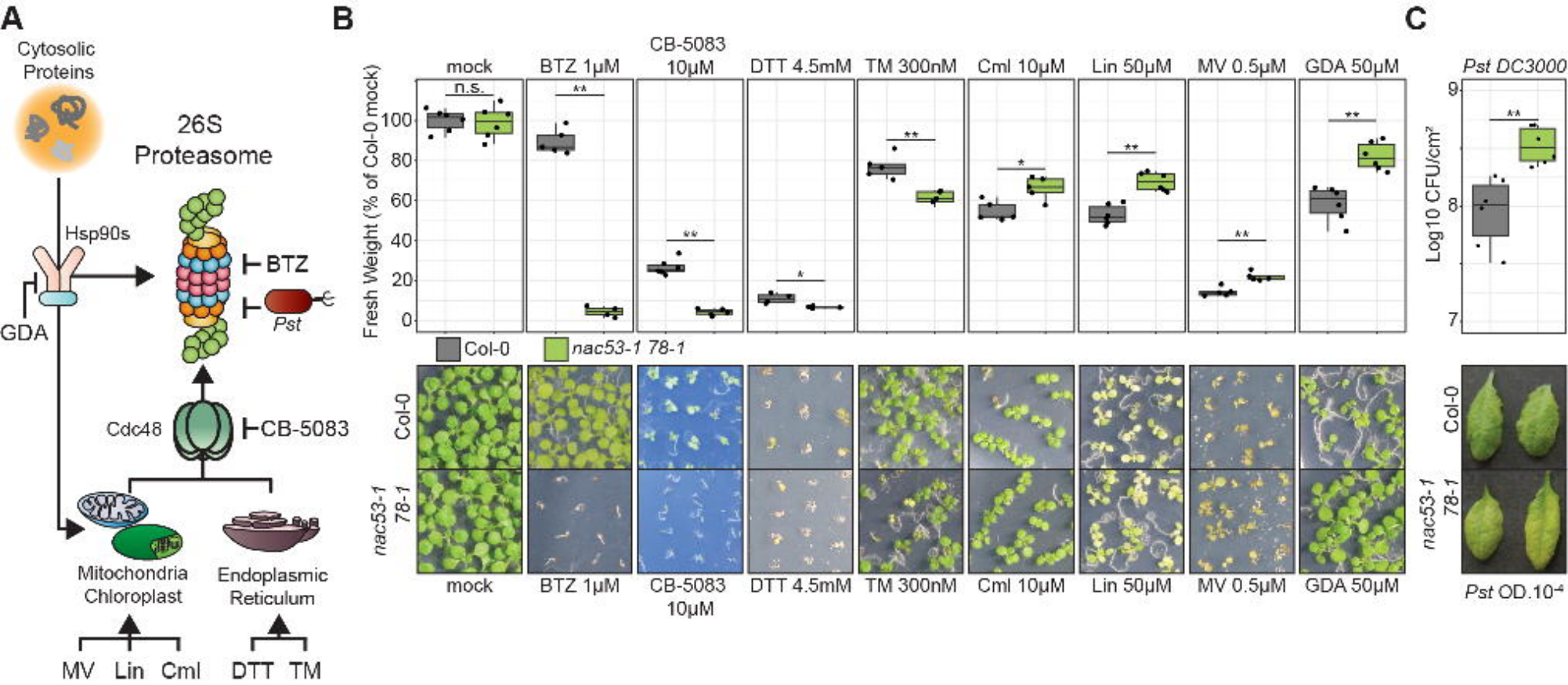
A
Cytosolic Proteins
26S Proteasome
Hsp90s
GDA
BTZ
Pst
Cdc48
CB-5083
Mitochondria Chloroplast
Endoplasmic Reticulum
MV Lin Cml
DTT TM
B
mock
BTZ 1µM
CB-5083 10µM
DTT 4.5mM
TM 300nM
Cml 10µM
Lin 50µM
MV 0.5µM
GDA 50µM
Fresh Weight (% of Col-0 mock)
n.s.
Col-0
nac53-1 78-1
C
Pst DC3000
Log10 CFU/cm²
Pst OD.10⁻⁴

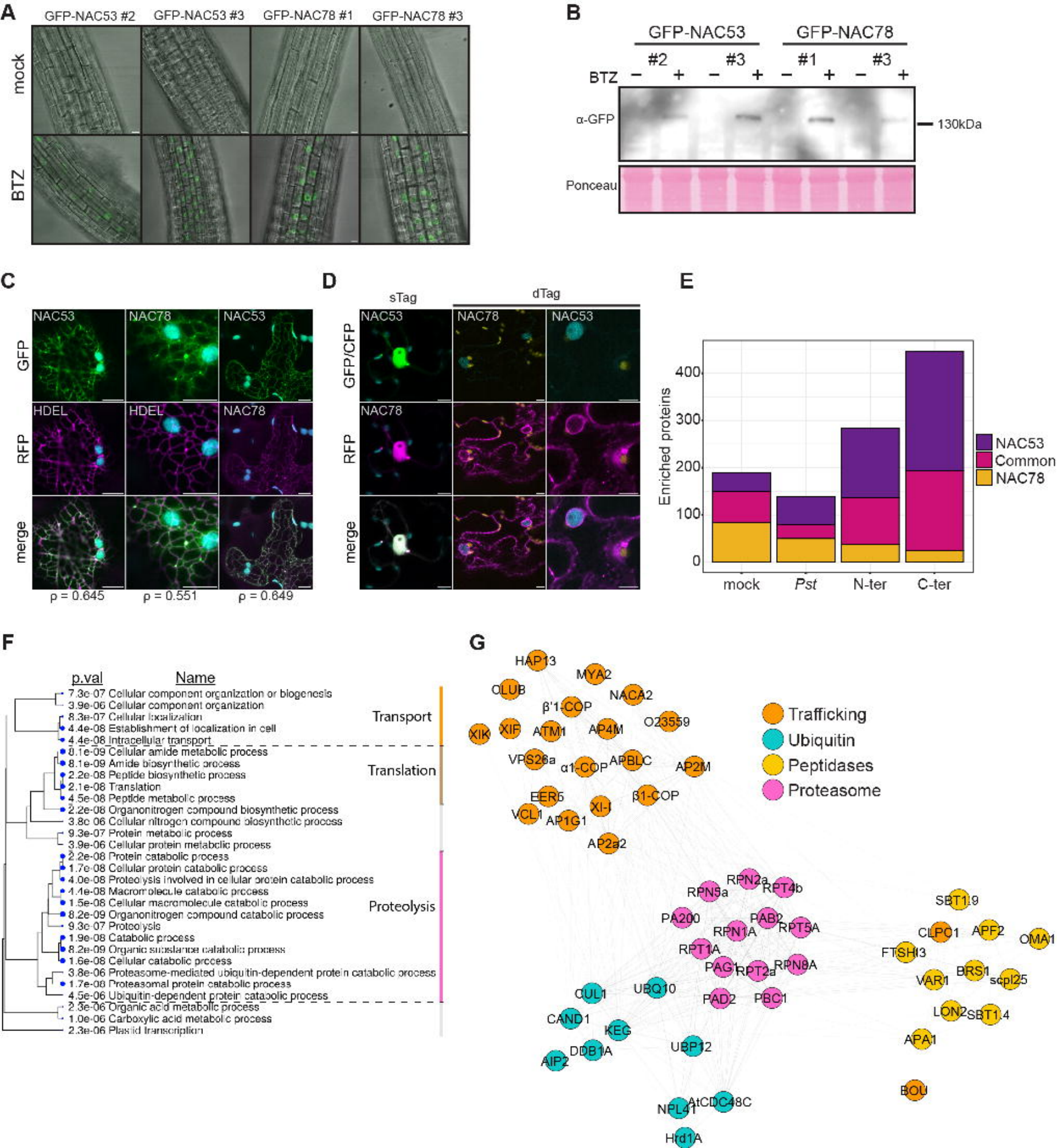
A
GFP-NAC53 #2
GFP-NAC53 #3
GFP-NAC78 #1
GFP-NAC78 #3
mock
BTZ
B
GFP-NAC53
GFP-NAC78
#2
#3
#1
#3
BTZ
α-GFP
130kDa
Ponceau
C
NAC53
NAC78
NAC53
HDEL
HDEL
NAC78
GFP
RFP
merge
ρ = 0.645
ρ = 0.551
ρ = 0.649
D
sTag
dTag
NAC53
NAC78
NAC53
NAC78
GFP/CFP
RFP
merge
E
Enriched proteins
400
300
200
100
0
mock
Pst
N-ter
C-ter
NAC53
Common
NAC78
F
p.val
Name
7.3e-07 Cellular component organization or biogenesis
3.9e-06 Cellular component organization
8.3e-07 Cellular localization
4.4e-08 Establishment of localization in cell
4.4e-08 Intracellular transport
8.1e-09 Cellular amide metabolic process
8.1e-09 Amide biosynthetic process
2.2e-08 Peptide biosynthetic process
2.1e-08 Translation
4.5e-08 Peptide metabolic process
2.2e-08 Organonitrogen compound biosynthetic process
3.8e-06 Cellular nitrogen compound biosynthetic process
9.3e-07 Protein metabolic process
3.9e-06 Cellular protein metabolic process
2.2e-08 Protein catabolic process
1.7e-08 Cellular protein catabolic process
4.0e-08 Proteolysis involved in cellular protein catabolic process
4.4e-08 Macromolecule catabolic process
1.5e-08 Cellular macromolecule catabolic process
8.2e-09 Organonitrogen compound catabolic process
9.3e-07 Proteolysis
1.9e-08 Catabolic process
8.2e-09 Organic substance catabolic process
1.6e-08 Cellular catabolic process
3.8e-06 Proteasome-mediated ubiquitin-dependent protein catabolic process
1.7e-08 Proteasomal protein catabolic process
4.5e-06 Ubiquitin-dependent protein catabolic process
2.3e-06 Organic acid metabolic process
1.0e-06 Carboxylic acid metabolic process
2.3e-06 Plastid transcription
Transport
Translation
Proteolysis
G
HAP13
MYA2
OLUB
NACA2
β'1-COP
O23559
XIK
XIF
ATM1
AP4M
VPS26a
α1-COP
APBLC
AP2M
EER5
β1-COP
XI-I
VCL1
AP1G1
AP2a2
Trafficking
Ubiquitin
Peptidases
Proteasome
RPN2a
RPN5a
RPT4b
PA200
PAB2
RPN1A
RPT5A
RPT1A
PAG1
RPT2a
RPN8A
CUL1
UBQ10
PAD2
PBC1
CAND1
KEG
DDB1A
UBP12
AIP2
NPL41
AtCDC48C
Hrd1A
SBT1.9
CLPC1
APF2
OMA1
FTSH13
BRS1
VAR1
scpl25
LON2
SBT1.4
APA1
BOU

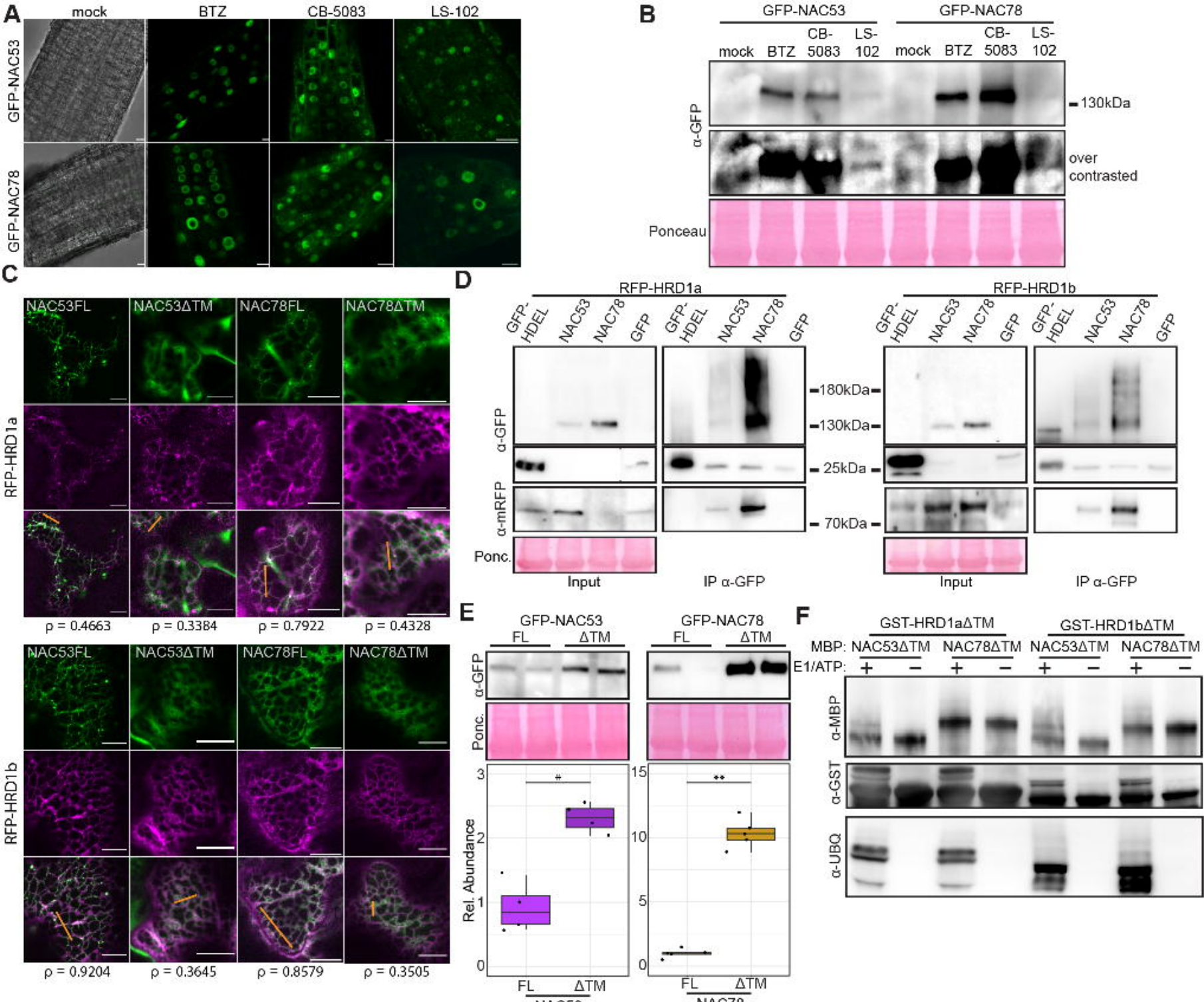
A
mock
BTZ
CB-5083
LS-102
GFP-NAC53
GFP-NAC78
B
GFP-NAC53
GFP-NAC78
mock
BTZ
CB-5083
LS-102
α-GFP
130kDa
over contrasted
Ponceau
C
NAC53FL
NAC53ΔTM
NAC78FL
NAC78ΔTM
RFP-HRD1a
ρ = 0.4663
ρ = 0.3384
ρ = 0.7922
ρ = 0.4328
RFP-HRD1b
ρ = 0.9204
ρ = 0.3645
ρ = 0.8579
ρ = 0.3505
D
RFP-HRD1a
RFP-HRD1b
GFP-HDEL
NAC53
NAC78
GFP
α-GFP
α-mRFP
Ponc.
180kDa
130kDa
25kDa
70kDa
Input
IP α-GFP
E
GFP-NAC53
GFP-NAC78
FL
ΔTM
α-GFP
Ponc.
Rel. Abundance
NAC53
NAC78
F
GST-HRD1aΔTM
GST-HRD1bΔTM
MBP:
NAC53ΔTM
NAC78ΔTM
E1/ATP:
α-MBP
α-GST
α-UBQ
G
ER Membrane
CDC48 complex
HRD1 complex
NAC53/78
ER-Associated Degradation
Nuclear Translocation
26S Proteasome
Nucleus

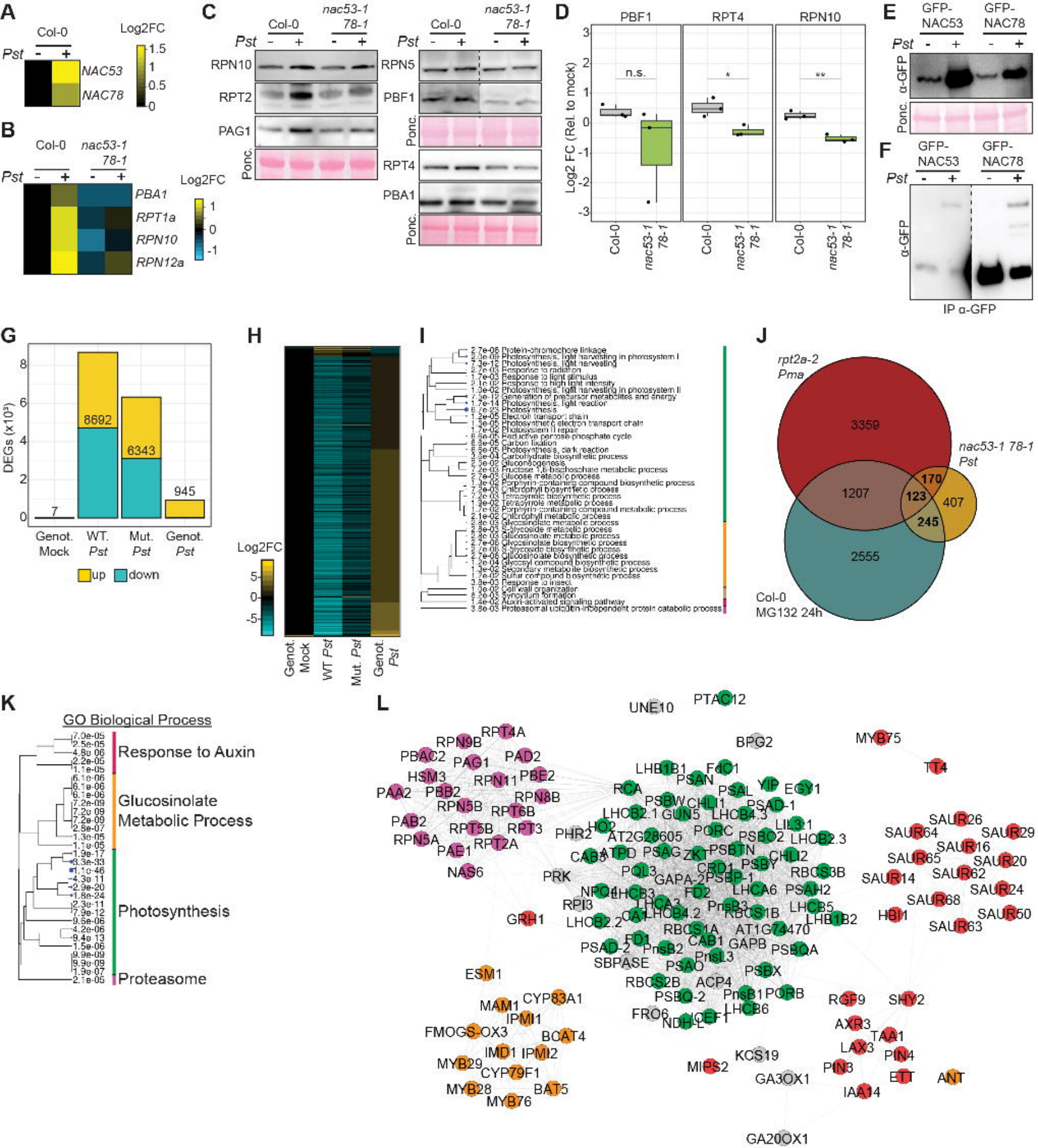
A
Col-0
Pst
-
+
NAC53
NAC78
Log2FC
1.5
1
0.5
0
B
Col-0
nac53-1
78-1
Pst
PBA1
RPT1a
RPN10
RPN12a
Log2FC
1
0
-1
C
Col-0
nac53-1
78-1
Pst
RPN10
RPT2
PAG1
Ponc.
RPN5
PBF1
RPT4
PBA1
D
PBF1
RPT4
RPN10
Log2 FC (Rel. to mock)
n.s.
*
**
Col-0
nac53-1
78-1
E
GFP-NAC53
GFP-NAC78
Pst
α-GFP
Ponc.
F
GFP-NAC53
GFP-NAC78
Pst
α-GFP
IP α-GFP
G
DEGs (x10³)
7
8692
6343
945
Genot. Mock
WT. Pst
Mut. Pst
Genot. Pst
up
down
H
Log2FC
5
0
-5
Genot. Mock
WT Pst
Mut. Pst
Genot. Pst
I
J
rpt2a-2 Pma
nac53-1 78-1 Pst
Col-0 MG132 24h
3359
1207
170
123
407
245
2555
K
GO Biological Process
Response to Auxin
Glucosinolate Metabolic Process
Photosynthesis
Proteasome
L
UNE10
PTAC12
RPT4A
RPN9B
PBAC2
PAG1
PAD2
HSM3
RPN11
PBE2
PAA2
PBB2
RPN8B
RPN5B
RPT6B
PAB2
RPT5B
RPT3
RPN5A
RPT2A
PAE1
NAS6
PRK
GRH1
BPG2
MYB75
TT4
LHB1B1
FdC1
PSAN
RCA
PSAL
YIP
EGY1
PSBW
CHL1
PSAD-1
LHCB2.1
GUN5
LHCB4.3
LIL3.1
PHR2
HO2
AT2G28605
PORC
PSBO2
LHCB2.3
CAB5
ATPD
PSAG
ZKT
PSBTN
CHL2
PQL3
CRD1
PSBY
RBCS3B
GAPA-2
PSBP-1
NPQ4
LHCB3
FD2
LHCA6
PSAH2
RPI3
LHCA3
PnsB3
LHCB5
CA1
LHCB4.2
RBCS1B
LHCB2.2
LHB1B2
RBCS1A
AT1G74470
FD1
CAB1
GAPB
PSAD-2
PnsB2
PSBQA
SBPASE
PnsL3
PSAO
PSBX
ESM1
RBCS2B
ACP4
PSBQ-2
PnsB1
PORB
LHCB6
FRO6
NDH-L
CYP83A1
MAM1
IPMI1
FMOGS-OX3
BCAT4
IMD1
IPMI2
MYB29
CYP79F1
MYB28
BAT5
MYB76
SAUR26
SAUR64
SAUR29
SAUR16
SAUR65
SAUR20
SAUR14
SAUR62
SAUR24
SAUR68
SAUR50
HBI1
SAUR63
RGF9
SHY2
AXR3
TAA1
LAX3
PIN4
KCS19
MIPS2
PIN3
ETT
ANT
GA3OX1
IAA14
GA20OX1

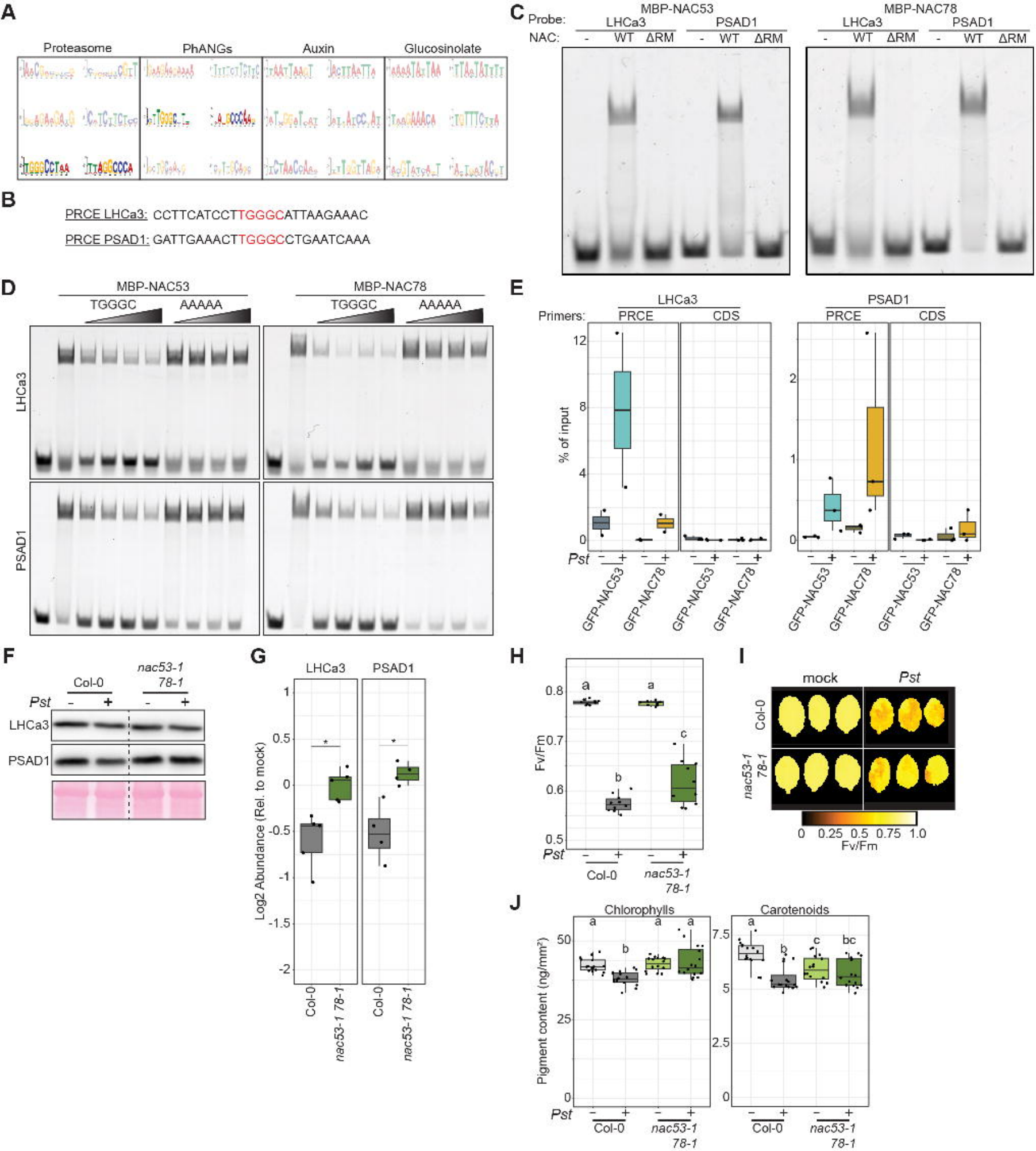
A
Proteasome
PhANGs
Auxin
Glucosinolate
B
PRCE LHCa3: CCTTCATCCTTGGGCATTAAGAAAC
PRCE PSAD1: GATTGAAACTTGGGCCTGAATCAAA
C
Probe:
MBP-NAC53
MBP-NAC78
LHCa3
PSAD1
NAC:
-
WT
ΔRM
D
MBP-NAC53
MBP-NAC78
TGGGC
AAAAA
LHCa3
PSAD1
E
Primers:
PRCE
CDS
% of input
Pst
GFP-NAC53
GFP-NAC78
F
Col-0
nac53-1
78-1
Pst
LHCa3
PSAD1
G
LHCa3
PSAD1
Log2 Abundance (Rel. to mock)
Col-0
nac53-1 78-1
H
Fv/Fm
Pst
Col-0
nac53-1
78-1
I
mock
Pst
Col-0
nac53-1
78-1
Fv/Fm
J
Chlorophylls
Carotenoids
Pigment content (ng/mm²)
Pst
Col-0
nac53-1
78-1